MOLECULAR BIOLOGY

N6-adenosine methylation of ribosomal RNA affects lipid oxidation and stress resistance

Noa Liberman[1,2]*, Zach K. O'Brown[1,2]*, Andrew Scott Earl[1,2]*, Konstantinos Boulias[1,2], Maxim V. Gerashchenko[3], Simon Yuan Wang[1,2], Colette Fritsche[1], Paul-Enguerrand Fady[1], Anna Dong[1], Vadim N. Gladyshev[3], Eric Lieberman Greer[1,2†]

During stress, global translation is reduced, but specific transcripts are actively translated. How stress-responsive mRNAs are selectively translated is unknown. We show that METL-5 methylates adenosine 1717 on 18*S* ribosomal RNA in *C. elegans*, enhancing selective ribosomal binding and translation of specific mRNAs. One of these mRNAs, CYP-29A3, oxidizes the omega-3 polyunsaturated fatty acid eicosapentaenoic acid to eicosanoids, key stress signaling molecules. While *metl-5*–deficient animals grow normally under homeostatic conditions, they are resistant to a variety of stresses. *metl-5* mutant worms also show reduced bioactive lipid eicosanoids and dietary supplementation of eicosanoid products of CYP-29A3 restores stress sensitivity of *metl-5* mutant worms. Thus, methylation of a specific residue of 18*S* rRNA by METL-5 selectively enhances translation of *cyp-29A3* to increase production of eicosanoids, and blocking this pathway increases stress resistance. This study suggests that ribosome methylation can facilitate selective translation, providing another layer of regulation of the stress response.

INTRODUCTION

Ribosomal modifications help specify which transcripts are translated under different environmental conditions (*1*, *2*), providing an additional layer of control to gene regulation. Ribosomal RNAs (rRNAs; 28*S*, 18*S*, 5.8*S*, and 5*S* in eukaryotes) are encoded by many copies of ribosomal DNA throughout the genome, which display tissue-specific expression patterns (*3*), raising the possibility that different combinations of rRNAs and ribosomal proteins could form ribosomes that are specialized for translation of subsets of mRNAs (*4*). rRNAs are heavily modified during production and maturation. Some of these modifications (2′-*O*-methylation and pseudouridinylation) occur in substoichiometric frequency (*5*), suggesting that specialized ribosomes might regulate differential translation of distinct transcripts. Ribosomes are bound to different transcripts in response to different stresses (*6*–*8*), and rRNA methylation has been shown to regulate ribosome assembly on a cohort of specific transcripts (*9*, *10*). However, which specific enzymes regulate rRNA methylation events, what the effects of each of these methylation events are, which specific transcripts are translated, and what the functional consequences of most of the rRNA modifications are remain unclear.

Fatty acids and their oxidized signaling molecules, termed eicosanoids, regulate many physiological processes, including inflammation (*11*), immune responses (*11*), embryo implantation (*12*), the perception of pain (*13*), cell growth (*14*), blood flow (*14*), and tumorigenesis (*14*). Whether rRNA methylation can control these physiological processes by regulation of fatty acid production and oxidation is unknown. Here, we identify METL-5 as a novel, highly specific 18*S* rRNA N6-methyladenosine (m^6A) methyltransferase of adenosine 1717. We find that METL-5 inhibits the stress response in *Caenorhabditis elegans* by selectively increasing the translation of CYP-29A3, a cytochrome P450 enzyme that oxidizes ω-3 polyunsaturated fatty acids (PUFAs) eicosapentaenoic acid (EPA) to eicosanoids that increase the lethality of stress in wild-type (WT) worms. Together, this work mechanistically demonstrates how the complexity of rRNA modifications can regulate specific stress responses.

[1]Division of Newborn Medicine, Boston Children's Hospital, 300 Longwood Avenue, Boston, MA 02115, USA. [2]Department of Pediatrics, Harvard Medical School, Boston, MA 02115, USA. [3]Division of Genetics, Department of Medicine, Brigham and Women's Hospital, Harvard Medical School, Boston, MA 02115, USA.
*These authors contributed equally to this work.
†Corresponding author. Email: eric.greer@childrens.harvard.edu

RESULTS

METL-5 methylates 18*S* rRNA on the N6 position of adenosine 1717 in vivo

To identify putative rRNA methyltransferases in *C. elegans*, we performed a directed RNA interference (RNAi) screen. We knocked down 13 genes with homology to the methyltransferase like (METTL) family, a family of proteins that methylate DNA and RNA in a variety of species (*15*). We then assessed general RNA methylation by mass spectrometry (MS). This approach will favor rRNA methylation given that >80% of the total RNA in a cell (*16*) is rRNA. We extracted RNA from worms fed with bacteria expressing an empty vector (E.V.) or double-stranded RNA against each of the 13 *METTL* genes. We performed ultrahigh-performance liquid chromatography (LC) coupled with triple quadrupole tandem MS (UHPLC-MS/MS) to look for changes in methylation of adenosine at the N6 position (m^6A) or cytosine at the N3 or C5 positions [N3-methylcytidine (m^3C) or C5-methylcytidine (m^5C), respectively] (Fig. 1A). Knockdown of C38D4.9/*metl-5*, a gene that has closest homology to human *Mettl5*, caused a ~40% decrease in m^6A levels in total RNA (Fig. 1B). To test whether the change in RNA m^6A methylation was due to *metl-5* knockdown rather than an off-target effect of the small interfering RNA, we examined RNA methylation in the two available *metl-5* mutant strains: strain tm4561, which contains a large deletion of exon 2 and also leads to a frame-shift, and strain gk747459, which contains a cytosine to thymine point mutation, which converts a glutamine to a stop codon immediately after the predicted catalytic domain of METL-5 (Fig. 1C). Both of these mutant strains displayed a ~50% reduction in m^6A levels in

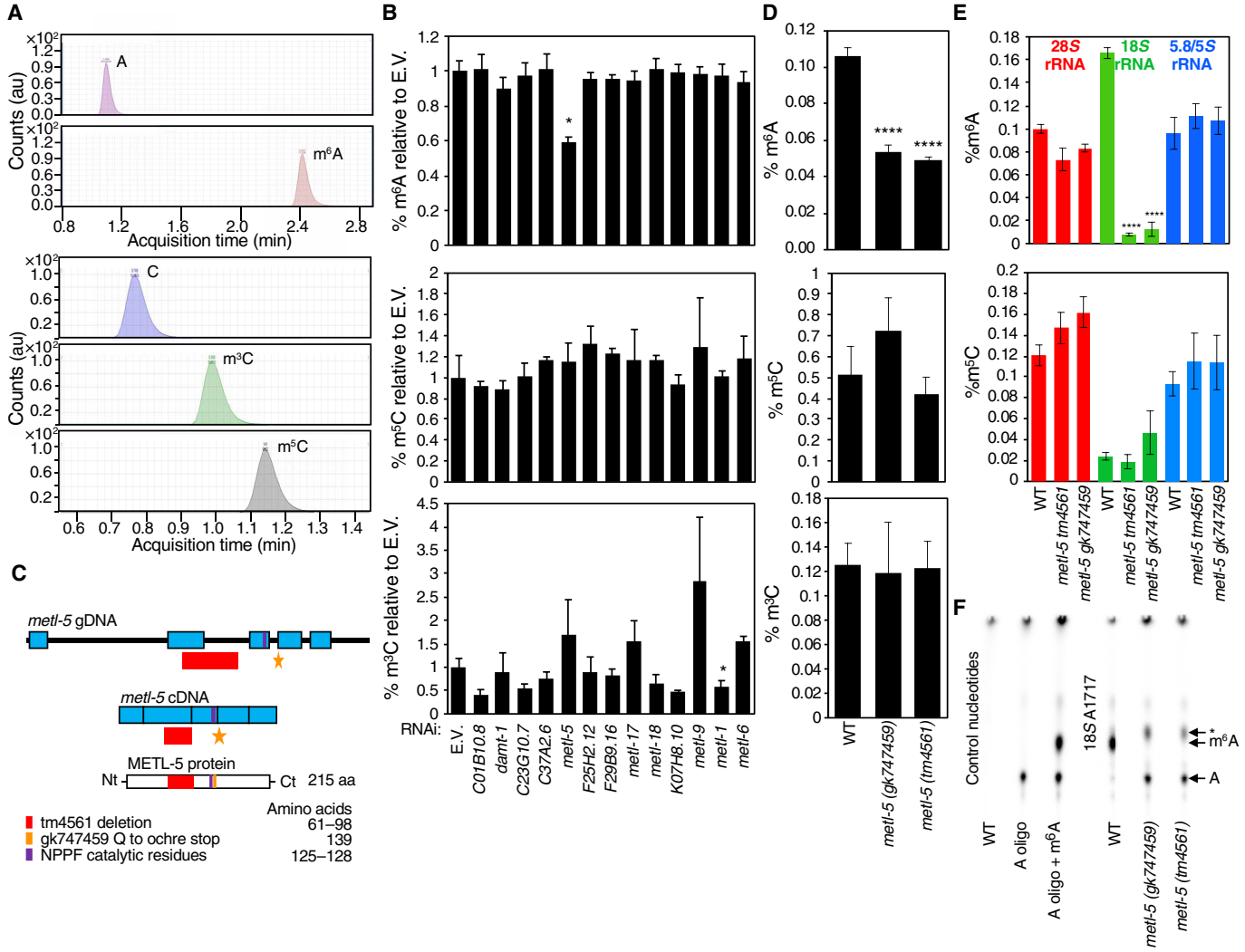

Fig. 1. METL-5 N6-methylates adenosine 1717 on 18*S* rRNA in vivo. (**A**) UHPLC-MS/MS chromatography peaks can distinguish adenosine from N6-methylated adenosine (m^6A) and cytidine from C3-methylated cytidine and C5-methylated cytidine based on retention time on the column. au, area units. (**B**) RNAi screen of 13 *metl* family members in *C. elegans* reveals that knockdown of *C38D4.9/metl-5* causes a decrease in m^6A levels on total RNA without any significant effects on m^5C or m^3C levels, as assessed by UHPLC-MS/MS. Each bar represents the mean ± SEM of two biological replicates performed in duplicate. *$P < 0.05$, as assessed by one-way analysis of variance (ANOVA). E.V., empty vector. (**C**) Schematic of *metl-5* genomic DNA (gDNA), cDNA, and protein indicating the location of the catalytic domain and the mutations used in this study. aa, amino acid; Nt, N terminus; Ct, C terminus. (**D**) Two *metl-5* mutant strains display decreases in m^6A levels without any change in m^3C or m^5C levels, as assessed by UHPLC-MS/MS. Each bar represents the mean ± SEM of 4 to 12 biological replicates performed in duplicate. ****$P < 0.0001$, as assessed by one-way ANOVA. (**E**) Two *metl-5* mutant strains display decreases in m^6A levels on purified 18*S* rRNA without changes in m^5C levels, as assessed by UHPLC-MS/MS. No detectable changes were observed in purified 28*S* or 5.8*S* and 5*S* in m^6A or m^5C. m^3C was undetectable in all rRNA purifications. Each bar represents the mean ± SEM of two to four biological replicates performed in duplicate. ****$P < 0.0001$, as assessed by one-way ANOVA. (**F**) Directed RNA cleavage, followed by ^{32}P labeling and thin-layer chromatography, demonstrates that adenosine 1717 on 18*S* rRNA is N6-adenosine methylated ~98% of the time in WT worms but is unmethylated in *metl-5* mutant worms. The left blot represents the migration of unmethylated adenosines and N6-methylated adenosines, and the right blot represents the methylation of adenosine 1717 in 18*S* rRNA. The asterisk (*) indicates a nonspecific spot migrating above the m^6A location.

total RNA with no discernable changes in m^5C and m^3C (Fig. 1D). These results suggest that both of these mutant strains are putative null *metl-5* strains and that METL-5 can methylate m^6A on RNA. Since rRNA makes up >80% of the total RNA in a cell (*16*), these results suggest that METL-5 methylates adenine on rRNA.

To determine which RNAs METL-5 modifies, we electrophoresed on agarose gels total RNA from WT and *metl-5* mutant worms to separate 28*S*, 18*S*, and 5.8*S*/5*S* rRNAs. mRNA was isolated by two successive rounds of polyadenylation selection, followed by rRNA depletion. We performed UHPLC-MS/MS on each population of RNA and found no discernable change in mRNA m^6A methylation (97% of WT; fig. S1A) or in m^6A levels on 28*S* or 5.8/5*S* rRNA in *metl-5* mutant strains (Fig. 1E). However, N6-adenosine methylation of 18*S* rRNA in both mutant strains was reduced by an order of magnitude compared to WT worms (Fig. 1E). To rule out the possibility that the change in 18*S* rRNA methylation could be due to contamination with bacterial 16*S* rRNA, we measured the degree of N6-adenosine methylation of bacterial 16*S* RNA (fig. S1B). Although total *Escherichia coli* RNA contained 0.35% m^6A, only 0.06% of bacterial 16*S* rRNA was methylated on adenosine, about a third of the

level in WT *C. elegans* 18*S* rRNA (Fig. 1E). Thus, any contaminating 16*S* rRNA in our 18*S* rRNA preparations would have a negligible effect on overall methylation levels. The decrease in 18*S* rRNA in *metl-5* mutant strains was specific to m^6A since m^5C levels on ribosomal subunits did not significantly change in the two mutant strains (Fig. 1E). A recent paper demonstrated that human METTL5 required a methyltransferase activator protein, TRMT112, to maintain stability (*17*). However, we found that knockdown of the TRMT112 ortholog, C04H5.1, had no effect on 18*S* rRNA m^6A levels (fig. S1C). Together, these data suggest that METL-5 controls 18*S* methylation on the N6 position of adenines.

18*S* rRNA has one known N6-adenosine methylation site in both *Xenopus laevis* (adenosine 1789) and *Homo sapiens* (adenosine 1832) (*18*). These sites correspond to adenosine 1717 in *C. elegans* 18*S* rRNA. This residue is predicted to interact with mRNA on the basis of its location in the crystal structure of *Thermus thermophilus* (*19*). However, this residue was reported to be unmodified in unicellular organisms (*20*). To test whether adenosine 1717 is methylated by METL-5 in *C. elegans*, 18*S* rRNA purified from WT and *metl-5* mutant worms was analyzed for methylation by directed RNA cleavage, followed by ^{32}P labeling and thin-layer chromatography (*21*). Adenosine 1717 on 18*S* rRNA was methylated ~98% of the time in WT *C. elegans* but was unmethylated in both *metl-5* mutant strains (Fig. 1F). Together, these data suggest that *metl-5* is responsible for the majority of 18*S* rRNA methylation at site 1717.

METL-5 directly methylates 18*S* rRNA on the N6 position of adenosine 1717

To determine whether METL-5 directly methylates 18*S* rRNA, we expressed a glutathione *S*-transferase (GST)–tagged *metl-5* in bacteria, purified METL-5 to a single band (Fig. 2A), and analyzed its ability to methylate 18*S* rRNA from *metl-5* mutant worms. Recombinant METL-5 methylated 18*S* rRNA from *metl-5* mutant, but not WT, worms, confirming that METL-5 is an 18*S* rRNA methylase that is active without any cofactors and that WT 18*S* rRNA is constitutively and uniformly methylated (Fig. 2B). To verify further that METL-5 is an 18*S* rRNA methylase, the putative catalytic site AspProProPhe (NPPF) sequence of METL-5 (*22*) was mutated to AlaProProAla (APPA). Mutation of the catalytic site to APPA ablated the N6-adenosine methyltransferase activity on 18*S* rRNA from *metl-5* mutant worms (Fig. 2B). To determine whether METL-5 could methylate adenosine 1717 within the 18*S* sequence, we performed in vitro methylation assays with recombinant METL-5 using 26- and 46-nucleotide synthetic oligonucleosides consisting of adenosine 1717 and flanking nucleosides from the 18*S* rRNA sequence (Fig. 2C). We found that WT, but not catalytically dead, METL-5 methylated both oligonucleosides. This methylation was specific to adenosine 1717, as there was no methylation detected in in vitro methylation assays using the same oligos where adenosine 1717 had been replaced by a guanosine (Fig. 2C).

metl-5 mutant worms are more resistant to a variety of stresses via a translation-dependent process

To identify the biological role of *metl-5*, we compared the life span of WT and *metl-5* mutant strains of *C. elegans*. Under normal growth conditions, *metl-5* mutant strains did not exhibit any gross morphological abnormalities and showed no significant difference in survival or fecundity compared to WT worms (Fig. 3A and table S1). *metl-5* mutant strains were also similarly susceptible to the pathogenic bacterium *Pseudomonas aeruginosa* (PA14) [*metl-5(gk747459)*, $P = 0.70$; *metl-5(tm4561)*, $P = 0.65$; fig. S2A and table S1] (*23*, *24*). However, *metl-5* mutants were more resistant to the oxidant paraquat (*N*,*N*′-dimethyl-4,4′-bipyridinium dichloride) [*metl-5(gk747459)*, $P = 0.01$; *metl-5(tm4561)*, $P < 0.01$; fig. S2B and table S1] (*25*), 37°C heat shock [$P < 0.05$ by one-way analysis of variance (ANOVA); *metl-5(gk747459)*, $P < 0.0001$; Fig. 3, B and C, and table S1], cold stress [*metl-5(gk747459)*, $P = 0.0013$; *metl-5(tm4561)*, $P = 0.009$; Fig. 3D and table S1] (*26*), ultraviolet (UV) irradiation [*metl-5(gk747459)*, $P < 0.0001$; *metl-5(tm4561)*, $P < 0.0001$; Fig. 3E and table S1] (*27*), and a combination of hypoxia and mild heat stress ($P < 0.0001$ by two-way ANOVA; fig. S2C) (*28*). To determine whether the increased survival in response to hypoxia and mild heat stress was due to resistance to hypoxia or heat stress or both, *metl-5* mutant worm survival to either stress was assessed independently (fig. S2, D to F). Mutant worms had no change in survival compared to WT worms after 6 days of growth at 0.1% oxygen (fig. S2D) or after 3 weeks of growth at mildly elevated temperatures (25° and 28°C) (fig. S2, E and F, and table S1), suggesting that they were only protected from the combined stress. In addition, we also found that *metl-5* mutant worms displayed increased survival after 37°C heat shock and UV irradiation not only when stressed at the L4 larval stage but also if the stress was applied immediately after reproduction stopped (day 7) or in middle age (day 10) (fig. S2, G and H). Unsurprisingly, as C04H5.1 knockdown had no effect on 18*S* rRNA m^6A methylation levels (fig. S1C), knockdown similarly had no effect on 37°C heat shock resistance (fig. S2I). Thus, *metl-5* mutant worms were resistant to a variety of stresses (oxidant, cold, heat shock, and UV irradiation) but were not more resistant to *P. aeruginosa* infection or milder heat stresses. To determine whether this increased stress resistance was due to METL-5 activity, we generated transgenic rescue strains of WT or APPA mutant *metl-5* driven by the ubiquitous *eft-3* promoter in a *metl-5(tm4561)* mutant background ($P_{eft\text{-}3}$*::metl-5* WT and $P_{eft\text{-}3}$*::metl-5 APPA*) (fig. S2J). Three independent $P_{eft\text{-}3}$*::metl-5 WT* lines but not three independent $P_{eft\text{-}3}$*::metl-5 APPA* lines rescued the 37°C heat shock and 18*S* rRNA m^6A levels compared to three independent control rescue lines (Fig. 3, F and G). These results indicate that METL-5 catalytic activity is required for both the 18*S* rRNA methylation and the stress resistance phenotype.

To investigate whether the increased stress resistance of *metl-5* mutant worms is due to changes in N6-adenosine methylation, we subjected WT worms to heat stress, paraquat, hypoxia, and starvation and measured the effects of stress on m^6A levels. None of these stresses had any discernable effect on m^6A levels in total RNA (fig. S3, A to D) or 18*S* rRNA (fig. S3, E to H). Similarly, heat stress had no discernable effect on m^6A levels or location, as assessed by immunofluorescence of whole worms (fig. S3, I and J). Thus, the increased stress resistance of *metl-5* mutant worms was unlikely to be due to stress-induced differences in 18*S* rRNA methylation.

Next, considering that this is a rRNA modification, we decided to explore the premise that increased stress resistance is dependent on translation. We examined the effect of cycloheximide (*29*), a translation inhibitor, on heat shock and UV irradiation resistance of *metl-5* mutant worms. Cycloheximide treatment eliminated the increased survival of *metl-5* mutant worms to heat shock and UV irradiation but had no effect on the survival of WT worms (Fig. 3, H and I). Thus, the beneficial effects of *metl-5* mutation seem to depend on translation.

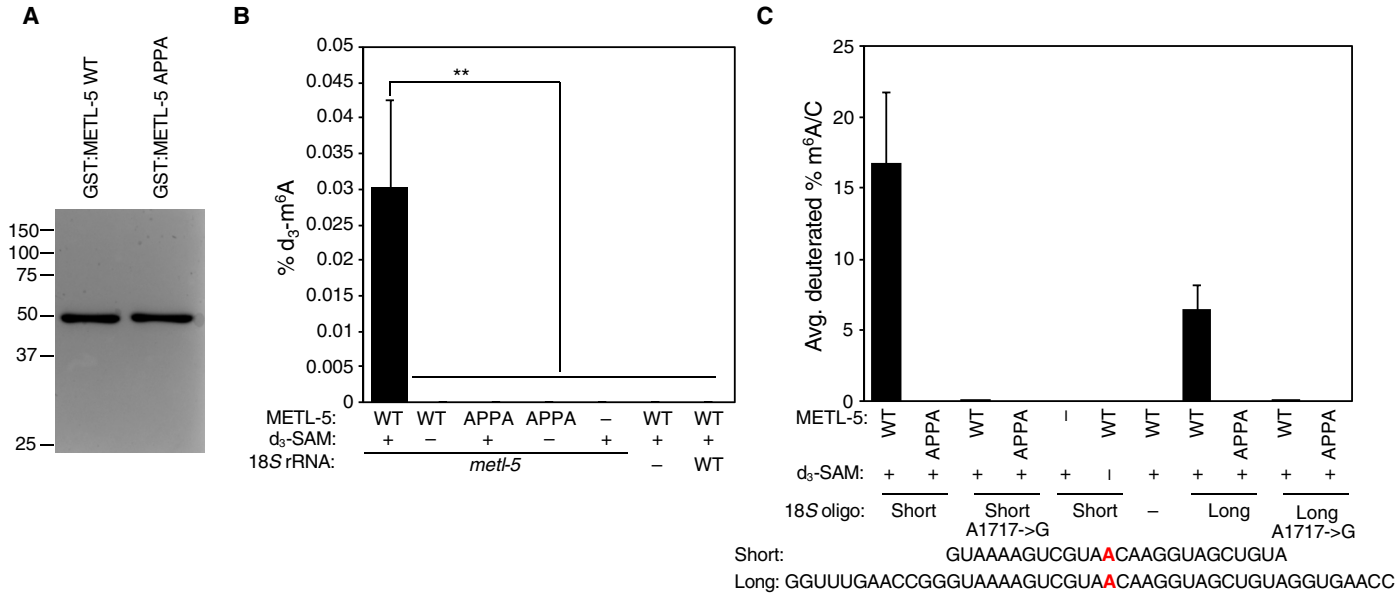

Fig. 2. METL-5 N6-methylates adenosine 1717 on 18*S* rRNA in vitro. (**A**) Coomassie staining of SDS–polyacrylamide gel electrophoresis (SDS-PAGE) gels reveals that GST-tagged METL-5 WT and APPA catalytic mutant proteins are pure and migrate at the same location. (**B**) WT GST-tagged METL-5, but not the catalytically inactive mutant APPA, is able to methylate 18*S* rRNA purified from *metl-5* mutant worms, as assessed by UHPLC-MS/MS of deuterated m^6A. METL-5 was unable to methylate 18*S* rRNA purified from WT worms, which are already fully methylated. Deuterated *S*-adenosyl methionine (d_3-SAM) was used as the methyl donor to ensure that methylation was added during methylation assays. Each bar represents the mean ± SEM of three independent experiments. $^{**}P < 0.005$, as assessed by one-way ANOVA with Tukey's multiple comparisons test. (**C**) WT GST-tagged METL-5, but not the catalytically inactive mutant APPA, is able to methylate both a short and a long oligo containing the sequence surrounding adenosine 1717 in 18*S* rRNA. This methylation is absent when the nucleoside representing adenosine 1717 is replaced with a guanosine despite the presence of additional adenosines. (Top) Each bar represents the mean ± SEM of three independent experiments, and (bottom) the oligo sequences are displayed with adenosine 1717 highlighted in red. Avg., average.

metl-5 mutant worms display reduced translation of the P450 gene *cyp-29A3*

We next sought to unbiasedly understand the translation-dependent mechanism responsible for increased stress resistance in *metl-5* mutant worms. Ribosome methylation has been proposed to regulate ribosomal binding to particular transcripts during specific conditions (*9*, *10*). To examine whether 18*S* rRNA N6-adenosine methylation alters translation, we evaluated ^{35}S-methionine incorporation into newly synthesized proteins in WT and *metl-5* mutant strains grown for 3 hours at 20° or 37°C (*30*). As expected, heat shock altered the pattern of translated proteins on SDS–polyacrylamide gel electrophoresis (SDS-PAGE) (Fig. 4A). However, no consistent difference in the profile of newly synthesized proteins, as assessed by phosphor imaging of ^{35}S incorporation, or in the total amount of synthesized protein, as assessed by scintillation counting, was apparent at either temperature in *metl-5* mutant relative to WT worms (Fig. 4, A and B). Similarly, although heat shock transitioned all ribosomes to monosomes, the polysome profile of *metl-5* mutant worms was similar to WT worms at both temperatures (Fig. 4C). Thus, 18*S* rRNA N6-adenosine methylation does not globally affect polysome profiles and the translation status in *C. elegans*. To determine whether 18*S* rRNA N6-adenosine methylation alters ribosome binding or association levels of specific transcripts, we sequenced ribosome-bound RNAs and total cellular polyadenylated selected RNA (*31*) in three independent biological replicates from WT and *metl-5* mutant worms grown at 20°C or heat-shocked at 37°C for 3 hours. We observed a high degree of variability in biological replicates, presumably due to slight differences in the cohorts of worms from experiment to experiment and the heterogeneity of RNAs in different cell types. Although heat shock caused marked shifts in which transcripts were translated and bound by ribosomes, *metl-5* mutation did not cause significant shifts in translation efficiency (Fig. 4D). We therefore examined actively translated transcripts in WT and *metl-5* mutant worms (Fig. 4E and fig. S4). Only a small number of transcripts were significantly changed in *metl-5* mutants compared to WT worms at either temperature. A single transcript, *cyp-29A3* encoding for a cytochrome P450 enzyme, stood out as greatly reduced (more than 10-fold) for ribosomal binding under both conditions in *metl-5* mutant worms compared to WT worms (Fig. 4F). Because of its relatively low abundance, *cyp-29A3* was excluded from our RNA sequencing analysis (fig. S5). We therefore performed quantitative real-time polymerase chain reaction (qRT-PCR) to directly examine the expression levels of *cyp-29A3*. We found that *cyp-29A3* displayed equal levels of expression at 20°C in WT and *metl-5* mutant worms, and *cyp-29A3*'s expression was elevated to an equivalent extent when heat-shocked at 37°C (Fig. 4G). Together, these data suggested that *cyp-29A3* has lower ribosome occupancy in *metl-5* mutant worms. To examine this more directly, we extracted RNA from polysome profile fractions of WT and *metl-5* mutant worms at 20° and 37°C and performed qRT-PCR of *cyp-29A3* and the control housekeeping gene *act-1*. We found that *act-1* distribution was similar between WT and *metl-5* mutant strains and did not change substantially with heat stress (fig. S4D). Conversely, *cyp-29A3* mRNA levels were higher in the polysome fractions after heat shock, indicating an increase in active translation of CYP-29A3. However, the levels of

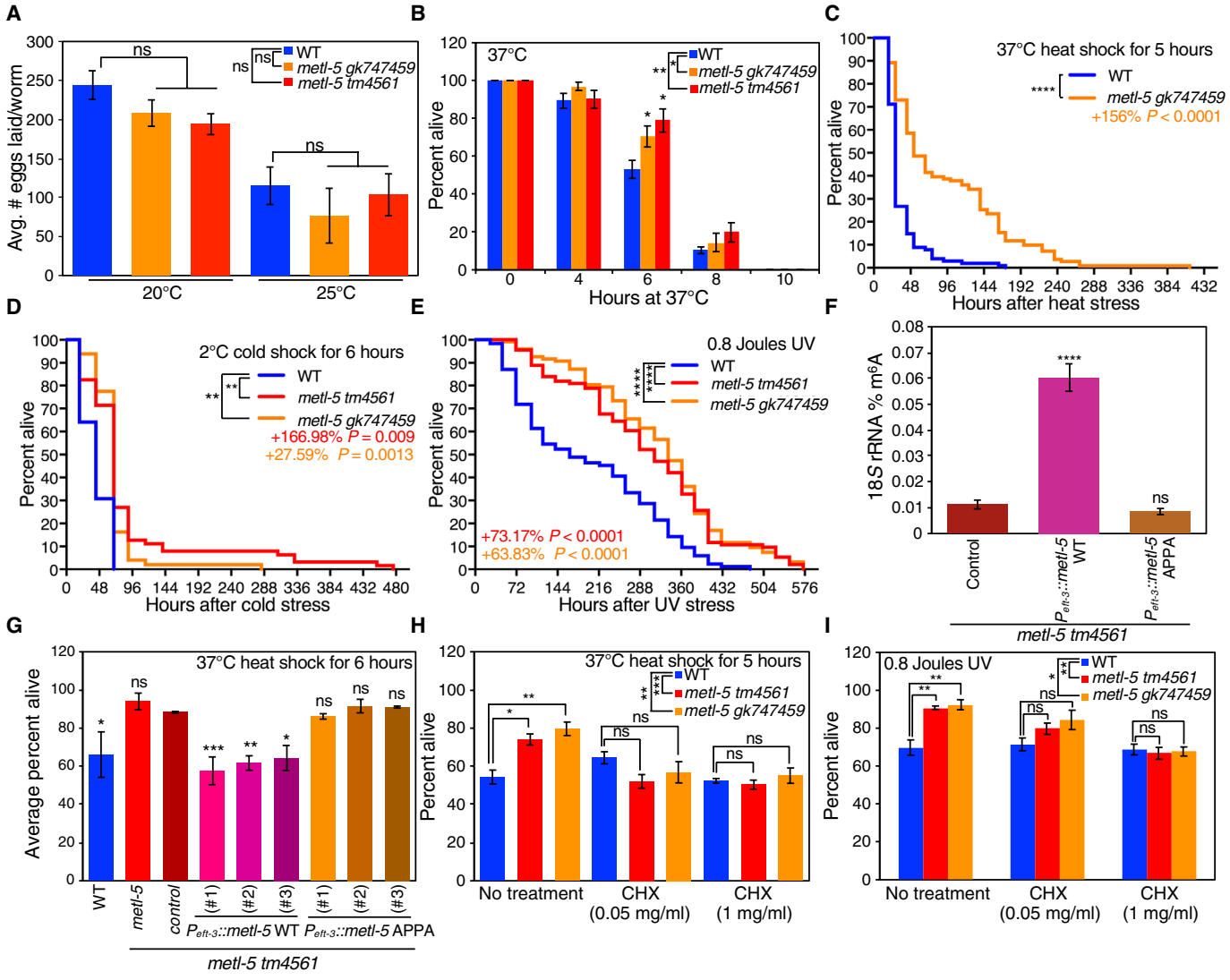

Fig. 3. *metl-5* mutant worms are resistant to several stresses. (**A**) Two *metl-5* mutant strains display a nonsignificant trend toward fewer progeny than WT worms grown at 20° or 25°C. Each bar represents the mean ± SEM of one to six independent experiments performed with three plates of 10 worms each. ns, not significant as assessed by two-way ANOVA and Tukey's multiple comparisons test of one-way ANOVA. (**B**) Two *metl-5* mutant strains display increased survival after L4 worms were placed at 37°C for the time indicated, then grown at 20°C, and assessed for survival after 24 hours. This graph represents the mean ± SEM of five independent experiments. Bar: $^{*}P < 0.05$, as assessed by unpaired *t* test, and $^{*}P < 0.05$ and $^{**}P < 0.005$, as assessed by two-way ANOVA. (**C**) *metl-5(gk747459)* mutant worms display a 156% increase in average life span relative to WT worms when L4 worms were exposed to a 37°C heat shock for 5 hours and then grown at 20°C for the remainder of the assay. This graph represents one experiment of five and was performed with three plates of at least 30 worms per plate. Statistics and replicate experiments are presented in table S1. $^{****}P < 0.0001$, as assessed by log-rank Mantel-Cox survival analysis. (**D**) Two *metl-5* mutant strains display increased survival after young adults were placed at 2°C for 6 hours before being returned to 20°C for the remainder of their life. This graph represents one experiment with three plates of 30 worms per plate, which was performed in triplicate. Statistics and replicate experiments are presented in table S1. $^{**}P < 0.005$, as assessed by log-rank Mantel-Cox survival analysis. (**E**) Two *metl-5* mutant strains display increased survival after young adults were exposed to 0.8 Joules and then grown at 20°C for the remainder of their life. This graph represents one experiment with three plates of 30 worms per plate, which was performed in triplicate. Statistics and replicate experiments are presented in table S1. $^{****}P < 0.0001$, as assessed by log-rank Mantel-Cox survival analysis. (**F**) *metl-5* WT but not the catalytically inactive mutant APPA overexpression lines in *metl-5(tm4561)* mutant worms rescues 18*S* rRNA m^6A methylation levels, as assessed by UHPLC-MS/MS. Each bar represents the mean ± SEM of two to three independent lines. $^{****}P < 0.0001$, as assessed by one-way ANOVA. Successful overexpression of *metl-5* was validated by real-time polymerase chain reaction (RT-PCR), as shown in fig. S2J. (**G**) The heat shock resistance phenotype of three independent *metl-5* WT but not the catalytically inactive mutant APPA overexpression lines in *metl-5(tm4561)* mutant worms reverts to the same levels as WT worms. Each bar represents the average ± SEM of three independent experiments performed with three plates of 20 to 50 worms each. The control represents three independent lines performed in three independent experiments in triplicate. Worms were treated with 37°C heat shock for 6 hours and then grown at 20°C and assessed for survival after 24 hours. $^{*}P < 0.05$, $^{**}P < 0.005$, and $^{***}P = 0.0005$, as assessed by one-way ANOVA relative to control-injected lines. (**H**) Increased heat shock survival of two *metl-5* mutant strains was eliminated by inhibition of translation by cycloheximide treatment. This graph represents the mean ± SEM of three independent experiments of three plates containing 20 to 35 worms each. Bar: $^{*}P < 0.05$ and $^{**}P < 0.005$, as assessed by Tukey's multiple comparisons test of one-way ANOVA analysis; strain: $^{**}P < 0.005$ and $^{***}P = 0.0005$, as assessed by two-way ANOVA. (**I**) Increased survival of two *metl-5* mutant strains exposed to 0.8 Joules was eliminated by inhibition of translation by cycloheximide treatment. This graph represents the mean ± SEM of three independent experiments of three plates containing 20 to 35 worms each. Bar: $^{**}P < 0.005$, as assessed by one-way ANOVA with Tukey's multiple comparisons test. $^{*}P < 0.05$ and $^{**}P < 0.005$, as assessed by two-way ANOVA.

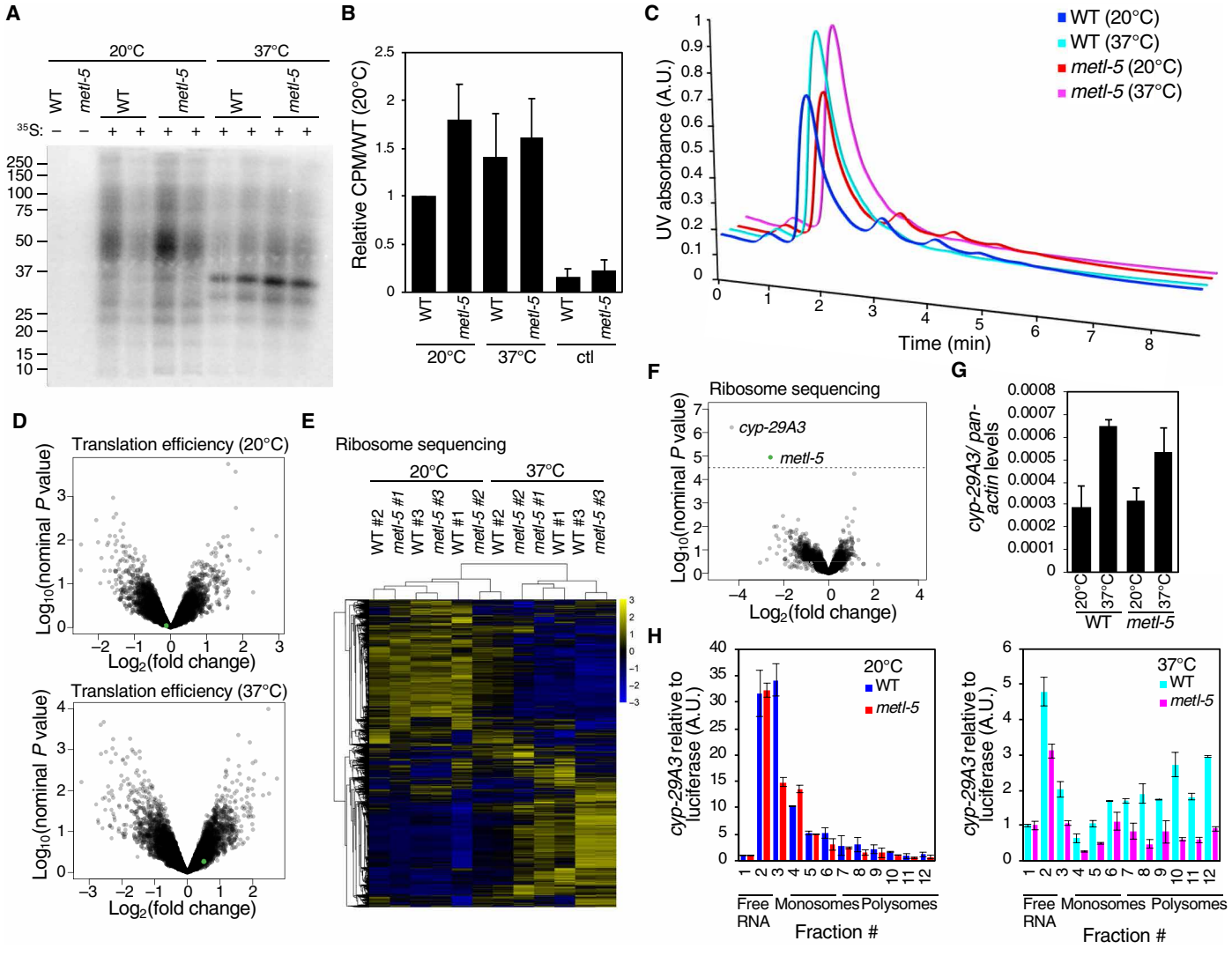

Fig. 4. *metl-5* has no global effect on translation but regulates ribosome occupancy of *cyp-29A3*. (**A**) The profile of newly translated proteins changes in *C. elegans* in response to 3 hours at 37°C, but this is unaffected by *metl-5(tm4561)* mutation, as assessed by phosphor imaging of ^{35}S incorporation. This blot is representative of three independent experiments. (**B**) Absolute ^{35}S incorporation was unaffected by 3 hours at 37°C or *metl-5(tm4561)* mutation, as assessed by scintillation counting. Control (ctl) lanes represent worms that were treated with ^{35}S-methionine for 1 min. Each bar represents the mean ± SEM of three independent experiments performed in duplicate. CPM, counts per minute. (**C**) Polysome profiles of *metl-5(tm4561)* mutant worms were indistinguishable from WT worms grown at 20°C or when profiles shifted to monosomes after 2 hours at 37°C. This graph is a representative experiment where UV absorbance at OD_{254} (optical density at 254 nm) is monitored continuously. (**D**) Volcano plot of translation efficiency as calculated by ribosome occupancy relative to mRNA transcript of WT and *metl-5(tm4561)* mutant worms grown at 20°C (top) or heat-shocked for 3 hours at 37°C (bottom) revealed no significant change in translation efficiency in mutant worms. (**E**) Ribosome sequencing clusters of WT and *metl-5(tm4561)* mutant worms grown at 20°C or heat-shocked for 3 hours at 37°C revealed global changes in transcripts bound by ribosomes in response to heat shock with no global change in response to *metl-5* mutation. (**F**) Volcano plot of ribosome sequencing reveals that ribosomes are significantly differentially bound to the normalized transcripts of only *cyp-29A3* and *metl-5* after correction for multiple hypothesis testing. Ribosome sequencing was normalized by values within the replicate. (**G**) *cyp-29A3* mRNA is at similar levels in WT and *metl-5* mutant worms grown at 20°C and is increased to a similar extent in WT and *metl-5* mutant worms in response to heat shock at 37°C for 5 hours. Each bar represents the mean ± SEM of two independent experiments performed in duplicate. (**H**) *cyp-29A3* mRNA is higher in polysome fractions after heat shock, but this increase is blunted in the *metl-5* mutant worms relative to WT worms, as assessed by polysome fractionation followed by qRT-PCR. *cyp-29A3* expressions relative to the spiked-in internal standard of firefly luciferase were examined at each fraction of the polysome profile by qRT-PCR of WT and *metl-5* mutant worms grown at 20°C (left) and 37°C for 5 hours (right). Relative expression is normalized to fraction #1 to demonstrate the relative change in mRNA presence. Fractions #1 and #2 represent the free RNA, fractions #4 to #6 represent the monosomes, and fractions #7 to #11 represent the polysomes.

cyp-29A3 mRNA were reduced in the heavier polysome fractions in the *metl-5* mutant strain relative to WT worms (Fig. 4H). These data therefore suggest that *cyp-29A3* is preferentially translated in response to heat stress, and this induction is blunted in *metl-5* mutant worms.

Eicosanoid synthesis, which *cyp-29A3* regulates, is reduced in *metl-5* mutant worms

The ω-3 and ω-6 fatty acids, α-linolenic acid and linoleic acid, respectively, are essential fatty acids, which humans cannot synthesize (*32*). α-Linolenic acid and linoleic acid are precursors for longer and

more unsaturated fatty acids, termed PUFAs, including the ω-3 PUFA EPA and the ω-6 PUFA arachidonic acid (AA) that increase cell membrane flexibility and selective permeability (*32*). These PUFAs are oxidized to create the signaling molecules termed eicosanoids, which include prostaglandins, thromboxanes, and leukotrienes (*33*). Some PUFAs are metabolized to eicosanoids by cytochrome P450 enzymes (*34*). *C. elegans* express all genes required for the synthesis of PUFAs (*32*) and 75 cytochrome P450 genes (*35*). CYP-29A3 oxidizes the omega-3 PUFA EPA to produce three types of eicosanoids termed epoxyeicosatetraenoic acids (EETs): 17,18-epoxy eicosatetraenoic acid (17,18-EpETE), 17,18-dihydroxyeicosa-5,8,11,14-tetraenoic acid (17,18-DiHETE), and 20-hydroxy-eicosapentaenoic acid (20-HEPE) (*35*). Eicosanoids are hormone-like signaling lipids implicated in a variety of processes including inflammation (*11*), embryo implantation (*12*), and tumorigenesis (*14*). In *C. elegans*, these three EETs play a role in pharyngeal pumping and food uptake (*36*). To determine whether the change in *cyp-29A3* accounts for the stress resistance of *metl-5* mutant worms, we examined the heat shock sensitivity of a genetic mutant strain of *cyp-29A3*, *gk827495*, in which tryptophan-89 is converted to an amber stop codon. *cyp-29A3* mutant worms at the L4 larval stage were more resistant to heat stress than WT worms ($P < 0.01$, by unpaired *t* test; Fig. 5A). We also found that *cyp-29A3* mutant worms displayed increased survival after 37°C heat shock immediately after reproduction stopped (day 7) and in middle age (day 10) (fig. S2G). Furthermore, *metl-5;cyp-29A3* double mutant worms did not survive any better than *metl-5* or *cyp-29A3* mutants alone (fig. S6A), suggesting that the products of these two genes act in the same pathway. To test whether CYP-29A3 expression was sufficient to rescue the *metl-5* stress-resistant phenotype, we generated transgenic rescue strains of *cyp-29A3* driven by the ubiquitous *eft-3* promoter in a *metl-5(tm4561)* mutant background ($P_{eft\text{-}3}$*::cyp-29A3*). Overexpression of *cyp-29A3* in three independent $P_{eft\text{-}3}$*::cyp-29A3* lines (fig. S6B) had no effect on 18*S* rRNA m^6A methylation levels, as assessed by UHPLC-MS/MS (fig. S6C); however, overexpression did rescue the 37°C heat shock resistance phenotype compared to three independent control rescue lines (Fig. 5B), indicating that CYP-29A3 is sufficient to rescue the stress resistance phenotype. Knockdown of *cyp-29A3* reduces levels of the lipid eicosanoid EETs 17,18-EpETE, 17,18-DiHETE, and 20-HEPE (*35*). To determine whether *metl-5* mutant worms, which show decreased ribosome occupancy on *cyp-29A3* mRNA (Fig. 4H), also have decreased lipid content, we stained *metl-5* mutant worms for total lipid content with Oil Red O (ORO) (*37*, *38*). *metl-5* and *cyp-29A3* mutant worms had decreased lipid abundance to a similar extent ($P < 0.0001$, by one-way ANOVA; Fig. 5C). Furthermore, to examine whether *metl-5* mutant worms specifically had decreased eicosanoid EETs synthesized by CYP-29A3, we compared eicosanoid levels in whole WT, *cyp-29A3*, and *metl-5* mutant worms by gas chromatography coupled with MS (GC-MS). *metl-5* and *cyp-29A3* mutant worms had significantly decreased levels of the 17,18-EpETE, 17,18-DiHETE, and 20-HEPE eicosanoid EETs (Fig. 5D and fig. S7, A and B), while *metl-5* mutant worms showed no change in EPA, AA, or other fatty acids (Fig. 5D and fig. S7C).

We hypothesized that the reduced *cyp-29A3* translation and CYP-29A3 synthesis of eicosanoids could lead to the increased heat stress resistance in *metl-5* mutant worms. To test whether changes in these eicosanoids were responsible for the increased heat stress resistance of *metl-5* and *cyp-29A3* mutant worms, the diets of WT, *cyp-29A3(gk827495)*, and *metl-5(gk747459)* mutant strains were supplemented with the CYP-29A3 substrates, the omega-6 and omega-3 PUFAs, AA or EPA, respectively, and the CYP-29A3 products, the eicosanoid EETs 17,18-EpETE, 17,18-DiHETE, and 20-HEPE. Although dietary supplementation of the CYP-29A3 PUFA substrates had no effect on heat shock resistance of WT, *cyp-29A3*, or *metl-5* mutant worms, addition of the CYP-29A3 products 17,18-EpETE, 17,18-DiHETE, and 20-HEPE reverted the heat shock resistance of *cyp-29A3* and *metl-5* mutant worms to that of WT worms after 5 hours of 37°C heat shock (Fig. 5, E and F). These results suggest that reduced eicosanoid synthesis by CYP-29A3 is responsible for the increased stress resistance of *metl-5* mutant worms.

DISCUSSION

Our study identified METL-5 as a novel 18*S* rRNA N6-adenosine methyltransferase at adenosine 1717 in vivo and in vitro. We found that this enzyme is important for modulating the stress response in *C. elegans*. We show that N6-adenosine methylation by METL-5 regulates the binding of ribosomes to the transcript of CYP-29A3, a cytochrome P450 enzyme that oxygenates EPA to produce eicosanoid EETs 17,18-EpETE, 17,18-DiHETE, and 20-HEPE, decreased levels of which are critical for the heat stress resistance of *metl-5* mutant worms (Fig. 5G). How eicosanoid EETs can regulate the heat stress response is still unknown. Because eicosanoids have been implicated broadly in acting as small-molecule signaling mediators for inflammation, tissue homeostasis, immunity, and cancer (*11*–*14*), it will be important in future studies to determine how these signaling lipids can regulate the stress response in *C. elegans*. In *C. elegans*, cytochrome P450 enzymes and eicosanoids have been implicated in regulating the response to hypoxia (*39*), pharyngeal pumping and food uptake (*36*), sperm guidance (*40*), germ cell death and sterility (*41*), development, dauer formation, and longevity (*42*–*44*).

The interesting finding that deletion of *metl-5* and *cyp-29A3* increased stress resistance raises the question as to what evolutionary pressure would cause *C. elegans* to retain this detrimental pathway. We hypothesize that antagonistic pleiotropy could explain this finding and that some beneficial consequences of suppressing this pathway will be revealed under alternative conditions, as has been seen in other examples in *C. elegans* (*45*).

Our work suggests that METL-5 regulates the translation of CYP-29A3 to control stress resistance. It is still unclear how, on a molecular level, 18*S* rRNA methylation could specifically regulate the translation of CYP-29A3. Whether the 18*S* rRNA methylated on adenosine 1717 or alternatively unmethylated uniquely interacts with *cyp-29A3* mRNA and other transcripts is still unclear. We also have not ruled out whether METL-5 could methylate other substrates that are much less abundant than 18*S* rRNA.

METTL5, the mammalian homolog of METL-5, was recently identified as an 18*S* rRNA methyltransferase in humans. Whether METTL5 methylates the same residue on the 18*S* and whether it plays a conserved role in regulating the stress response and translation of cytochrome P450 enzymes remain to be seen. Human METTL5 seems to require binding of the methyltransferase activator TRMT112 to be stabilized (*17*). However, we found that the worm ortholog of TRMT112, C04H5.1, was dispensable for METL-5 stability and activity. Whether an alternative binding protein is required for METL-5 activity in *C. elegans* remains to be seen.

rRNA modifications provide a rich new layer of regulation of translation, and it will be exciting in the future to determine the

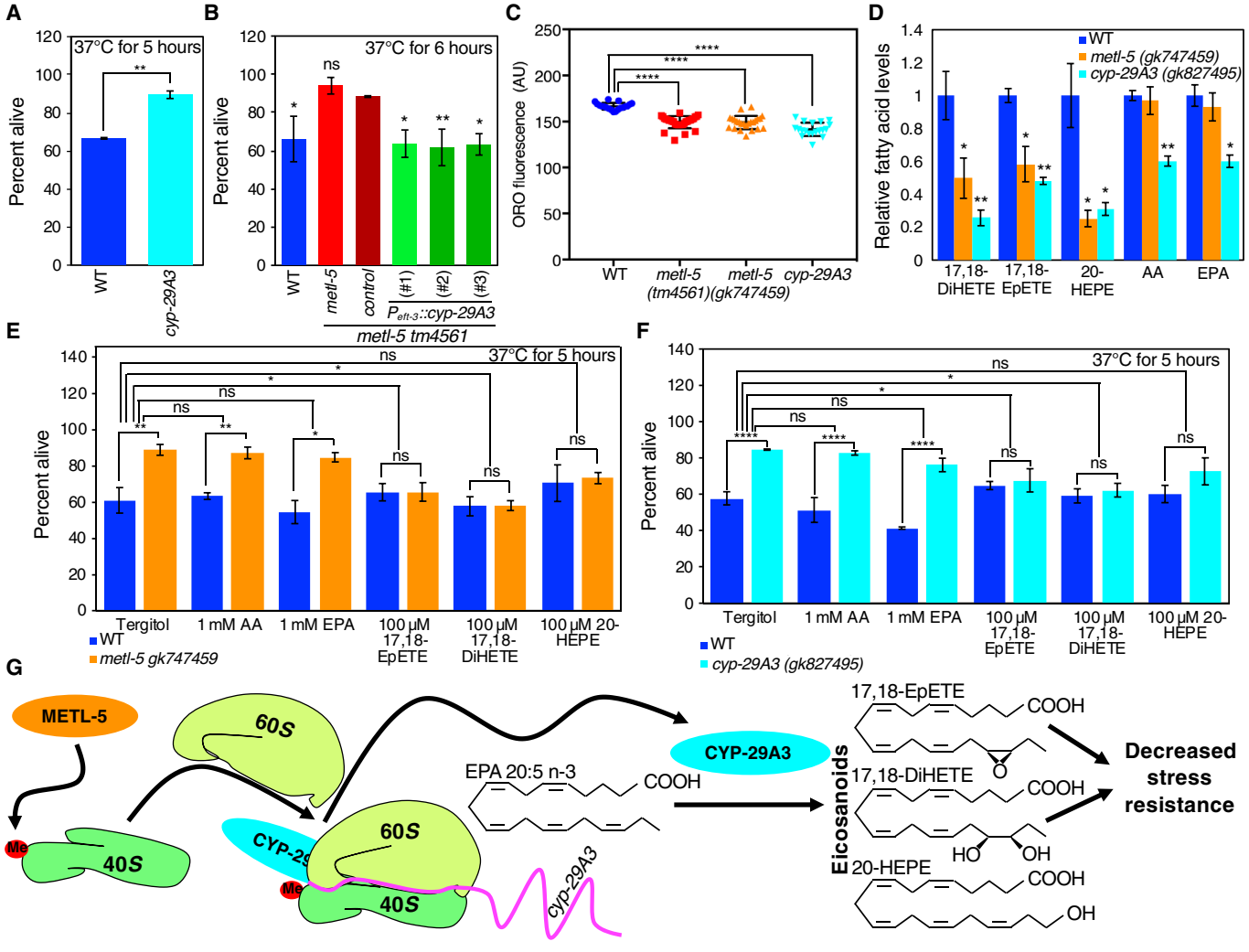

Fig. 5. *cyp-29A3* and EPA derivatives mediate heat stress resistance of *metl-5* mutant worms. (**A**) *cyp-29A3* mutant worms display increased stress resistance relative to WT worms after 5 hours of 37°C heat shock. Each bar represents the mean ± SEM of two independent experiments of three plates containing 20 to 35 worms each. $^{**}P < 0.01$, as assessed by unpaired *t* test. (**B**) The heat shock resistance phenotype of three independent *cyp-29A3* driven by the ubiquitous promoter of *eft-3* but not control lines in *metl-5(tm4561)* mutant worms reverts to the same levels as WT worms. Each bar represents the average ± SEM of three independent experiments performed with three plates of 20 to 50 worms each. The control represents three independent lines performed in three independent experiments in triplicate. Worms were treated with 37°C heat shock for 6 hours, then grown at 20°C, and assessed for survival after 24 hours. $^{*}P < 0.05$ and $^{**}P < 0.005$, as assessed by one-way ANOVA relative to control-injected lines. Note that the WT, *metl-5*, and control-injected strains are the same as in Fig. 3G, as these experiments were performed together. Successful overexpression of *cyp-29A3* was validated by qRT-PCR, as shown in fig. S6B. (**C**) *metl-5* and *cyp-29A3* mutant worms have lower lipid concentrations. as assessed by ORO fluorescence. Each column represents the mean ± SD of quantification of 19 to 30 worms each. $^{****}P < 0.0001$, as assessed by one-way ANOVA with Dunnett's multiple comparisons test. (**D**) *metl-5(gk747459)* and *cyp-29A3(gk827495)* mutant worms display lower levels of eicosanoid EETs 17,18-EpETE, 17,18-DiHETE, and 20-HEPE than WT worms, as assessed by GC-MS. *metl-5(gk747459)* mutant worms have equivalent levels of PUFAs AA and EPA compared to WT worms, but *cyp-29A3* mutant worms display lower levels of these PUFAs. Each bar represents the mean ± SEM of three independent experiments of ~6000 larval stage L4 worms each. $^{*}P < 0.05$ and $^{**}P < 0.01$, as assessed by Dunnett's multiple comparisons test of one-way ANOVA. (**E**) Dietary supplementation with eicosanoid EETs 17,18-EpETE, 17,18-DiHETE, and 20-HEPE reverts the increased stress resistance of *metl-5(gk747459)* mutant worms, but supplementation with AA or EPA does not cause a significant reversion of the increased stress resistance of *metl-5(gk747459)* mutant worms after 5 hours of 37°C heat shock. Each column represents the mean ± SEM of three to five independent experiments of three plates containing 20 to 54 worms each. $^{*}P < 0.05$ and $^{**}P < 0.01$, as assessed by multiple *t* tests and two-way ANOVA. (**F**) Dietary supplementation with eicosanoid EETs 17,18-EpETE, 17,18-DiHETE, and 20-HEPE reverts the increased stress resistance of *cyp-29A3(gk827495)* mutant worms, but supplementation with AA or EPA does not cause a significant reversion of the increased stress resistance of *cyp-29A3(gk827495)* mutant worms after 5 hours of 37°C heat shock. Each column represents the mean ± SEM of three independent experiments of three plates containing 20 to 54 worms each. $^{*}P < 0.05$ and $^{**}P < 0.01$, as assessed by multiple *t* tests and two-way ANOVA. (**G**) The model depicts how METL-5 can methylate the 18*S* rRNA of the 40*S* ribosomal subunit, which regulates binding to *cyp-29A3* transcripts, which, in turn, controls the oxidation of EPA to eicosanoid EETs, which regulate stress resistance in *C. elegans*.

extent to which these heavily modified RNAs can help specify appropriate translation. Two different methylations of 28*S* rRNA, N6-adenosine methylation of adenosine 4220 (*46*) and C5 cytosine methylation of cytosine 2381 (*10*), have been shown to affect polysome profiles, affect translation of specific mRNAs, and regulate cell proliferation and tumorigenesis (*46*) or longevity (*10*), highlighting the regulatory capacity of rRNA methylation for determining specific cellular responses. Further studies will be required to determine

how these rRNA methylation events can specify the ribosome to a distinct subset of target messenger RNAs. While more experiments are required to identify how 18*S* rRNA N6-adenosine methylation regulates ribosome occupancy on *cyp-29A3* mRNA and how the reduced eicosanoids in *metl-5* mutant worms control the heat stress response, the conservation of adenosine 1717 methylation on 18*S* rRNA and the eicosanoid synthesis pathway between worms and mammals suggest that this signaling pathway could regulate stress responses in other species, including mammals.

MATERIALS AND METHODS

Strains used and RNAi

The N2 Bristol strain was used as the WT background. Worms were grown on *dam*$^{-}$*dcm*$^{-}$ bacteria [New England Biolabs (NEB), C2925] on standard nematode growth medium (NGM) plates (*47*) in all experiments save for RNAi experiments. Bacteria expressing double-stranded RNA of METTL family members and C04H5.1 were obtained from the Ahringer and Vidal libraries (a gift from T. K. Blackwell). Bacteria were grown at 37°C and seeded on NGM plates containing ampicillin (100 mg ml^{-1}) and isopropylthiogalactoside (IPTG; 0.4 mM). Each vector was sequenced to verify the presence of the appropriate gene of interest. *metl-5(tm4561)* and *metl-5(gk747459)* strains were backcrossed six to eight times. The *cyp-29A3(gk827495)* strain was backcrossed two to seven times.

Single-worm genotyping

Single worms were placed in 5 μl of worm lysis buffer [50 mM KCl, 10 mM tris (pH 8.3), 2.5 mM $MgCl_2$, 0.45% NP-40, 0.45% Tween 20, 0.01% gelatin (w/v), and proteinase K (60 mg ml^{-1})] and incubated at −80°C for 1 hour, 60°C for 1 hour, and then 95°C for 15 min. PCRs were performed using the following primers: metl-5 tm4561 (forward), 5′-GTGGAATAATTTCCTCAAATGTGCTCTGAG-3′; metl-5 tm4561 (reverse), 5′-ACAGCCACGTCGAATGTGCC-3′; metl-5 gk747459 (forward), 5′-GGCTCAAAATGTGGAGTTAGAAACTACAG-3′; metl-5 gk747459 (reverse), 5′-CAACTCCGTCCCATTTCTTTGC-3′; *cyp-29A3* (forward), 5′-TCAGTGAAGCGGTAGAGAAAGGTC-3′; and *cyp-29A3* (reverse), 5′-AATCGTTGAAAAACTCATAGGGTCC-3′. PCRs for *metl-5(gk747459)* were digested with HpyCH4V to distinguish WT from mutant genotype, and PCRs for *cyp-29A3* were digested with Hae III to distinguish WT from mutant genotype. PCRs were performed according to the manufacturer's protocol (Invitrogen, Platinum PCR SuperMix), and PCRs were resolved on agarose gels.

UHPLC-MS/MS methods

Total RNA was extracted by the addition of 1 ml of TRIzol (Invitrogen) to 100 μl of young adult worms. Six freeze-thaw cycles were performed in liquid nitrogen. The RNA extraction was performed according to the TRIzol protocol (Invitrogen) or by the Direct-zol RNA kit (Zymo). To isolate 28*S*, 18*S*, and 5.8*S*/5*S* rRNAs, total RNA was electrophoresed on agarose gels to separate rRNAs, which were excised and purified using Zymoclean Gel RNA Recovery Kit (Zymo). Polyadenylated RNA was isolated from total RNA with two rounds of purification using Dynabeads mRNA Purification Kit (Invitrogen), following the manufacturer's instructions, and subsequently, any residual rRNAs were depleted using the NEBNext rRNA Depletion Kit (NEB), following the manufacturer's instructions. To quantify the concentrations of m^6A, m^3C, and m^5C in *C. elegans* RNA samples, we used pure nucleosides of adenosine (A), cytidine (C), m^6A, m^3C, or m^5C as calibration standards. For digestion to nucleosides, 250 ng to 1 μg of RNA samples were denatured at 95°C for 5 min and digested with 20 U of S1 nuclease (Thermo Fisher Scientific) at 37°C for 2 hours, followed sequentially by dephosphorylating with 2 U of FastAP thermosensitive alkaline phosphatase for 1 hour (Thermo Fisher Scientific) or digested with Nucleoside Digestion Mix (NEB, M069S) for 1 hour at 37°C. Digested RNA samples or pure nucleoside standards were diluted to 100 μl with double-distilled water and filtered through 0.22-μm Millex Syringe Filters. Five microliters of the filtered solution was injected for LC-MS/MS analysis and analyzed using the Agilent 1290 UHPLC system with a C18 reversed-phase column (2.1 mm by 50 mm; 1.8 m). Mobile phase A consisted of water with 0.1% (v/v) formic acid, and mobile phase B consisted of methanol with 0.1% (v/v) formic acid. MS detection was performed using an Agilent 6470 triple quadrupole mass spectrometer in positive electrospray ionization mode, and data were quantified in dynamic multiple reaction monitoring mode by monitoring the mass transitions 268➔136 for adenosine (A), 282➔150 for m^6A, 244➔112 for cytidine (C), and 258➔126 for m^3C and m^5C. The ratio of methylated A (%m^6A) or C (%m^3C or m^5C) in RNA samples was quantified using calibration curves from serial dilutions of the pure ribonucleoside standards.

Ribonuclease H site-specific cleavage directed by 2′-*O*-methyl RNA-DNA chimeras

18*S* RNA was subjected to ribonuclease H (RNase H) site-specific cleavage directed by 2′-*O*-methyl RNA-DNA chimeras. Gel-purified 18*S* RNA (300 ng) was mixed with 5 pmol chimeric oligo in 30 mM tris-Cl (pH 7.5) in a total volume of 5 μl. The resulting mixture was heated for 3 min at 95°C, followed by cooling to room temperature for 3 min. RNase H (5 U; NEB), recombinant shrimp alkaline phosphatase (1 U; NEB), and RNasin (20 U; Promega) were added in a total volume of 10 μl in 1× T4 polynucleotide kinase (PNK) buffer (NEB), and the mixture was incubated for 1 hour at 44°C, followed by heat inactivation for 5 min at 75°C. Radioactive end-labeling was performed with the addition of T4 PNK (20 U; NEB) and 2 μl of [γ-^{32}P]ATP (adenosine triphosphate) (6000 Ci/mmol) at 37°C for 1 hour in a total volume of 20 μl in 1× T4 PNK buffer, followed by heat inactivation for 5 min at 75°C. The free [γ-^{32}P]ATP was removed by the use of Bio-Spin 6 column (Bio-Rad) according to the manufacturer's instructions. The radioactive-labeled 18*S* fragments were subjected to tris-borate EDTA (TBE)–urea gel electrophoresis, followed by staining with SYBR Gold. The band that corresponded to the 38–base pair (bp) 5′ end-radiolabeled 3′ half 18*S* RNA fragment was excised, and RNA was eluted for 1 hour at 37°C in 300 μl of RNA extraction buffer [300 mM sodium acetate (pH 5.5), 1 mM EDTA, and 0.25% (v/v) SDS], followed by ethanol precipitation. The purified RNA was resuspended in diethyl pyrocarbonate–treated water and was digested with Nuclease P1 (2 U; Wako, USA) in 10 mM ammonium acetate (pH 5.2) and 2 mM $ZnCl_2$ for 2 hours at 60°C in a total volume of 20 μl. Digested nucleotide mixture (2.5 μl) was analyzed by thin-layer chromatography on a glass-backed polyethylenimine-cellulose plate (Merck Millipore) in a buffer containing isopropanol/HCl/water (70:15:15). Signal acquisition and quantification of the radiolabeled adenosine and m^6A were carried out using a BAS storage phosphor screen (GE Healthcare Life Sciences) at 200-μm resolution using the ImageQuant TL software (GE Healthcare Life Sciences).

Methyltransferase assays

The coding sequence of *metl-5* was cloned as an in-frame fusion to the GST-tagged vector pGEX-4T1. The catalytic site was mutated through site-directed mutagenesis. The recombinant proteins were expressed in *E. coli* BL21. Overnight induction of protein expression was carried out with 1 mM IPTG at 18°C. Bacteria were harvested at 4000 rpm and 4°C and resuspended in 10 ml of protein purification lysis buffer [50 mM tris-HCl (pH 7.5), 0.25 M NaCl, 0.1% Triton X-100, 1 mM phenylmethylsulfonyl fluoride, 1 mM dithiothreitol (DTT), and protease inhibitors]. After freezing the pellet at −80°C for 1 hour, the lysate was sonicated with a Bioruptor for 5 min on high level with 30-s on and 30-s off. Proteins were purified with Glutathione Sepharose 4B beads (GE Healthcare). Proteins and beads were washed three times with protein purification lysis buffer before incubating the beads with elution buffer [12 mg/ml; glutathione (GoldBio) in protein purification lysis buffer (pH 8.0)] for 30 min. Eluates were dialyzed overnight at 4°C with dialysis buffer [50 mM tris-HCl (pH 8.0), 1 mM EDTA, 1 mM DTT, and 20% glycerol]. Bradford assays and SDS-PAGE gel electrophoresis, followed by Coomassie staining, were performed to determine integrity and quantity of purified proteins.

In vitro methylation reactions assaying METL-5 activity against 18*S* rRNA purified from *metl-5* mutant worms were performed in a buffer containing 50 mM tris (pH 8.0), 1 mM EDTA, 1 mM DTT, 5% glycerol, 160 μM d_3-S-adenosyl methionine (SAM) using 200 nM GST–METL-5 protein, and 0.5 to 2 μg of 18*S* rRNA for 1 hour at 37°C. Then, reactions were incubated for 20 min at 65°C, followed by clean up and buffer exchange with Bio-Spin P-30 columns (Bio-Rad). RNA was digested to nucleosides with 20 U of S1 nuclease (Thermo Fisher Scientific) at 37°C for 2 hours, followed by treatment with Fast Alkaline Phosphatase (Thermo Fisher Scientific) for 1 hour at 37°C. Samples were diluted two times with Milli-Q water, and 5 μl was used for UHPLC-MS/MS analysis. Similar reactions were performed with synthesized 18*S* RNA oligos of the following sequences:

short 18*S* A1717, GUAAAAGUCGUAACAAGGUAGCUGUA; short 18*S* A1717->G, GUAAAAGUCGUAGCAAGGUAGCUGUA; long 18*S* A1717, GGUUUGAACCGGGUAAAAGUCGUAACAAGGUAGCUGUAGGUGAACC; and long 18*S* A1717->G, GGUUUGAACCGGGUAAAAGUCGUAGCAAGGUAGCUGUAGGUGAACC.

Transgenic strain creation

Expression vectors for creating transgenic strains were based on pSD1 plasmid vector (a gift from W. Mair and S. Dutta) that contains the ubiquitous *eft-3* promoter and *unc-54* 3′ untranslated region. *metl-5* and the *metl-5* APPA catalytic mutant were amplified from the pGEX-4T1 constructs and *cyp-29A3* from cDNA, followed by restriction-free cloning into the pSD1. Germline transformation experiments were performed as described (*48*). For the *metl-5* rescue experiments, injection mixes contained pSD1::*metl-5* or pSD1::*metl5* APPA plasmids at 50 ng/μl, pTG96 (20 ng/μl; $P_{sur\text{-}5}$::*gfp*) as a cotransformation marker, and 1-kb DNA ladder (80 ng/μl; Invitrogen) as carrier DNA. For the overexpression of *cyp-29A3* in *metl-5 (tm4561)*, the injection mix contained pSD1::*cyp-29A3* at 5 ng/μl, pTG96 (20 ng/μl; $P_{sur\text{-}5}$::*gfp*) as a cotransformation marker, and 1-kb DNA ladder as carrier DNA (80 ng/μl). For the control lines, the injection mix contained pTG96 (20 ng/μl; $P_{sur\text{-}5}$::*gfp*) as a cotransformation marker and 1-kb DNA ladder (80 ng/μl) as carrier DNA.

Longevity assays

Worm life-span assays were performed at 20°, 25°, and 28°C. Worm populations were synchronized by placing young adult worms on NGM plates seeded with *dam*$^-$*dcm*$^-$ bacteria for 6 hours and then removed. The hatching day was counted as day 1 for all life-span measurements. Worms were changed every other day to new plates to eliminate confounding progeny and were marked as dead or alive. Worms were scored as dead if they did not respond to repeated prods with a platinum pick. Worms were censored if they crawled off the plate or died from vulval bursting. For each life-span assay, ~90 worms were used in three plates (30 worms per plate). The data were plotted with the Kaplan-Meier survival curves, and statistical significance was determined by log-rank (Mantel-Cox) tests. Life-span assays were repeated at least once and showed similar trends in relative life-span effects. Representative Kaplan-Meier survival curves are shown in fig. S2 (D and E). Means, SEMs, and *P* values are shown in table S1.

PA14

NGM plates (35 mM) with 0.35% peptone rather than 0.25% peptone were spotted with 15 μl of PA14 from overnight cultures. This was spread over the entire plate. Worms were plated at the L4 stage on three plates per condition with 30 worms per plate (90 worms per assay). They were grown at 25°C and assessed every 6 to 12 hours for survival as in (*24*).

Paraquat

L4 or young adults were synchronized as described in the longevity assay, and five to seven worms were placed in 96-well plates in sextuplicate (at least 40 worms) in S medium containing 200 mM methyl viologen dichloride hydrate (paraquat). Worms were probed with a platinum pick every 45 min and were scored as alive as in the longevity assay in (*49*).

UV stress assays

Young adults were synchronized as described in the longevity assay on three plates per condition with 30 worms per plate (90 worms per assay). They were exposed to 0.8 J, then grown at 20°C, assessed every 24 hours for survival, scored as alive as in the longevity assay in (*27*).

Cold shock assays

Young adults were synchronized as described in the longevity assay on three plates per condition with 30 worms per plate (90 worms per assay). They were placed at 2°C for 6 hours and then assessed every 12 to 24 hours for survival and were scored as alive as in the longevity assays in (*26*). Note that a large number of the worms were censored because of bagging in these experiments. Censored worms were included in the statistical tests but were excluded from the figure shown in Fig. 3D.

Hypoxia and heat stress assays

Gravid day 1 adults were synchronized as described in the longevity assay on three plates per condition with 30 worms per plate (90 worms per assay). Replicate plates were prepared for six time points (0, 24, 48, 72, 96, and 120 hours) and left to grow at 28°C and 0.1% O_2 for the indicated length of time before being allowed to recover for 24 hours at 20°C and scored as alive as in the longevity assay. This is an adaptation of the protocol used in (*28*).

Heat stress assays

Synchronized L4 worms were placed at 37°C for the time indicated and then grown at 20°C for the remainder of the assay. Survival was assessed every 6 to 24 hours. For cycloheximide treatment, cycloheximide was diluted to 1 or 0.05 mg/ml (*29*), and 100 μl of cycloheximide was added on top of spotted food and allowed to soak in for 1 hour before synchronized L4 worms were placed on plates. Worms were allowed to crawl on plates for 45 min before they were placed at 37°C for 5 hours and returned to 20°C for the remainder of the assay. Survival was assessed after 24 hours.

Whole-mount immunocytochemistry

For whole-worm immunostaining, worms were washed several times to remove bacteria, resuspended in fixing solution [160 mM KCl, 40 mM NaCl, 20 mM Na_2EGTA, 10 mM spermidine HCl, 30 mM Pipes (pH 7.4), 50% methanol, 2% β-mercaptoethanol, and 2% formaldehyde], and subjected to two rounds of snap-freezing in liquid N_2. The worms were fixed at 4°C for 30 min and washed two times briefly in T buffer [100 mM tris-HCl (pH 7.4), 1 mM EDTA, and 1% Triton X-100] before a 1-hour incubation in T buffer supplemented with 1% β-mercaptoethanol at 37°C. The worms were washed with borate buffer [25 mM H_3BO_3 and 12.5 mM NaOH (pH 9.5)] and then washed in 1× phosphate-buffered saline (PBS) to equilibrate pH for RNase treatment. Worms were incubated at 37°C with a 1:100 RNase A/T1 Mix (Thermo Fisher Scientific) in PBS for 2 hours. Worms were washed in borate buffer and then incubated in borate buffer containing 10 mM DTT for 15 min. Worms were washed with borate buffer and then incubated in borate buffer containing 0.3% H_2O_2. Worms were washed in borate buffer briefly, blocked in PBST [PBS (pH 7.4), 1% bovine serum albumin, 0.5% Triton X-100, 5 mM sodium azide, and 1 mM EDTA] for 1 hour, and incubated overnight with α6mA antibody (1:100 in PBST; Synaptic Systems, 202 003). Worms were washed four times for 25 min in PBST and then incubated with Alexa Fluor 588 secondary antibody (1:50 in PBST). Worms were washed four times for 25 min in PBST. 4′,6-Diamidino-2-phenylindole (2 mg ml^{-1}) was added to visualize nuclei. The worms were mounted on a microscope slide and visualized using a Zeiss LSM 700 confocal system.

Fertility assays

From days 3 to 8 after hatching, 10 worms were placed on NGM plates with $dam^{-}dcm^{-}$ bacteria in triplicate (30 worms total per condition). Worms were grown at 20° or 25°C as indicated. After 24 hours, the adult worms were removed from each plate and placed on a new plate. The numbers of eggs and hatched worms on the plate were counted. Statistical analyses of fertility were performed using *t* tests using mean and SE values.

^{35}S-methionine feeding experiments

Bacteria were heat-shocked at 70°C for 30 min to kill the bacteria and prevent the bacteria from producing any ^{35}S-labeled proteins. ^{35}S-methionine (10 μCi; PerkinElmer) was added to 100 μl of heat-killed bacteria per condition. L4-staged WT and *metl-5(tm4561)* mutant worms were grown in mixture of heat-killed bacteria with ^{35}S-methionine at 20° or 37°C while shaking for 3 hours. As a negative control, WT and *metl-5(tm4561)* mutant worms were grown for 1 min in mixture of heat-killed bacteria with ^{35}S-methionine. Worms were washed four times in M9 buffer (22 mM KH_2PO_4, 34 mM K_2HPO_4, 86 mM NaCl, and 1 mM $MgSO_4$), followed by one wash in 70% ethanol and two additional washes in M9 buffer. Worm lysis buffer [115 μl; 20 mM $NaPO_4$, 150 mM NaCl, 1% NP-40, 0.5% sodium deoxycholate (DOC), 0.5% SDS, and 2 mM EDTA] was added to each sample, and they were flash-frozen in liquid N_2. Six freeze-thaws were performed in liquid N_2, and samples were placed in a Bioruptor for 5 min with 30-s on and 30-s off. Protein concentration was calculated by performing a Bradford assay, and equivalent concentrations of protein were placed in scintillation vials for measuring the translation of newly synthesized proteins. Samples were also run on SDS-PAGE gels, and gels were fixed in 30% (v/v) methanol and 10% glacial acetic acid while rocking at room temperature for 1 hour. Gels were washed two times in methanol for 45 min before briefly washing with water and drying the gels on Whatman paper. Newly synthesized proteins were detected by exposure of dried gels to phosphor screen for 2 weeks, followed by Storm phosphor imaging. Each experiment was performed with duplicate samples in triplicate.

Polysome profiling and qRT-PCR

Worms were synchronized by bleaching, and L4 worms were flash-frozen. Worm pellets were lysed and homogenized in lysis buffer [20 mM tris-HCl (pH 7.5), 100 mM KCl, 5 mM $MgCl_2$, cycloheximide (50 μg/ml), 1 mM DTT, protease and phosphatase cocktails (Sigma-Aldrich), 1% Tween 20, and 0.25% DOC] using pellet pestles for 1.7-ml tubes. SUPERase-In (Invitrogen) was added to each sample at 1 U/μl. RNA (~320 μg/ml) was loaded on a sucrose gradient (10 to 50%) prepared in SW 41 ultracentrifuge tubes (Beckman) using the Biocomp Gradient Maker. Samples were centrifuged for 2 hours at 39,000 rpm at 4°C in a SW 41 rotor (Beckman). Gradients were profiled at 1 ml/min using the Brandel gradient fractionation system coupled with the Bio-Rad UV detector, which continually monitored OD_{254} (optical density at 254 nm) values.

For qRT-PCR from polysome fractions, RNA (~160 to 800 μg/ml) was loaded on the sucrose gradients. One milliliter of fractions was collected every minute and flash-frozen. Equal volumes were taken from each fraction for RNA extraction and supplemented with a spike-in of 50 pg of firefly luciferase RNA (Promega). RNA was extracted using TRIzol LS and Direct-zol RNA MiniPrep Plus kit (Zymo). Eluted RNA was precipitated with the addition of GlycoBlue (Invitrogen) as a carrier. Equal volumes were taken for reverse transcription using SuperScript III First-Strand Synthesis System (Invitrogen). qRT-PCR was performed using iTaq Universal SYBR Green Supermix on a CFX real-time detection system (Bio-Rad). The results were expressed as $2^{[-(\text{gene of interest number of cycles} - \text{firefly luciferase number of cycles})]}$ using the following primers: *cyp-29A3* (forward), CCACCTGCTCATCCGATTTTTG; *cyp-29A3* (reverse), TGACCTTTCTCTACCGCTTCACTG; FLuc (forward), CGAGGGGGATGATAAACCGG; FLuc (reverse), CCAGATCCACAACCTTCGCT; *act-1* (forward), ACGACGAGTCCGGCCCATCC; and *act-1* (reverse), GAAAGCTGGTGGTGACGATGGTT.

Ribosome profiling

Ribosome profiling was performed according to published protocol (*50*) with modifications according to published protocols (*51*). Flash-frozen worm pellets were lysed and homogenized in lysis buffer [20 mM tris-HCl (pH 7.5), 100 mM KCl, 5 mM MgCl2, cycloheximide (50 μg/ml), 1 mM DTT, protease and phosphatase cocktails (Sigma-Aldrich), 1% Tween 20, and 0.25% DOC] using pellet pestles for 1.7-ml tubes. SUPERase-In (Invitrogen) was added to each sample at 1 U/μl.

Ten percent of each lysate (used for total RNA extraction and mRNA sequencing) was flash-frozen in 1 ml of TRIzol LS (Invitrogen). Lysate (~320 μg/ml) was incubated at 23°C for 1 hour with RNase T1 (20 U/~40 μg). Treated lysates were run on sucrose gradients (10 to 50%), and the monosome peak was collected. RNA from the monosome fraction was extracted using TRIzol LS and a Direct-zol kit (Zymo). The RNA was loaded on a Novex 15% TBE-urea gel (Life Technologies), and a fragment between 26 and 33 bp was excised and extracted from the gel. The library was prepared using the TruSeq Small RNA kit (Illumina) according to published protocol (*50*). The PCR product was then loaded on a Novex 6% TBE gel (Life Technologies), and a band around 150 bp was excised from the gel. The DNA was eluted from the gel and sent for quality assurance and sequencing at the Bauer Core Facility at Harvard University. RNA for mRNA sequencing was extracted using Direct-zol and sent for polyadenylate selection, library preparation, and sequencing at Novogene.

Transcriptome and ribosome profiling sequencing and analysis

Transcriptomes and ribosome profiling libraries were sequenced on the Illumina NovaSeq 6000 and NextSeq 500 platforms. mRNA libraries were sequenced in a paired-end mode with each read being 150 nucleotides long. Ribosome profiling libraries were sequenced in a single-end mode with 51-nucleotide read length before adapter trimming. Adapters were removed with Cutadapt software (*52*), and short read alignment and counting were performed with STAR aligner (*53*). Differential gene expression was evaluated with the DESeq2 package in the R programming environment (*54*). Gene set enrichment analysis (GSEA) was done with GSEA stand-alone software [Broad Institute; (*55*)] using a collection of *C. elegans* gene lists derived from the gene2go annotation data at the National Center for Biotechnology Information (NCBI). They are analogous to the Gene Ontology–based series of human-only collections available from the Molecular Signatures Database, a source gene list collection used in the original implementation of GSEA software by Broad Institute. Detailed analytical pipeline and all custom scripts are openly available on GitHub (https://github.com/germaximus/Liberman_2019). Raw data and gene counts tables are available from the NCBI Gene Expression Omnibus repository under accession number GSE131269.

Quantitative real-time polymerase chain reaction

Five hundred worms were synchronized by egg laying and grown to the L4 stage at 20°C. Worms were washed three times with M9 buffer (22 mM KH_2PO_4, 34 mM K_2HPO_4, 86 mM NaCl, and 1 mM $MgSO_4$). Worm pellets were resuspended in TRIzol (Invitrogen), followed by six freeze-thaw cycles in liquid N_2. The RNA extraction was performed according to the TRIzol protocol or Direct-zol RNA kit (Zymo). Total RNA (500 ng to 1 μg) was reverse-transcribed using the SuperScript III kit (Invitrogen), followed by quantitative PCR analysis on a Bio-Rad CFX96 RT-PCR system and C1000 Touch Thermal Cycler with SYBR Green Master Mix (Bio-Rad) with the following primers: *pan-actin* (forward), TCGGTATGGGACAGAAGGAC; *pan-actin* (reverse), CATCCCAGTTGGTGACGATA; *cyp-29A3* (forward), CCACCTGCTCATCCGATTTTTG; *cyp-29A3* (reverse), TGACCTTTCTCTACCGCTTCACTG; *cyp-29A3* (forward 2), TCAGTGAAGCGGTAGAGAAAGGTC; *cyp-29A3* (reverse 2), CGTTGAAAAACTCATAGGGTCCACC; *act-1* (forward), ACGACGAGTCCGGCCCATCC; *act-1* (reverse), GAAAGCTGGTGGTGACGATGGTT; *metl-5* (forward), CGGCCTGGTGGAAGTGTATT; *metl-5* (reverse), GGTAGTTGCCACCGCATTTC; *metl-5* (forward 2), ACATTCGACGTGGCTGTCAT; and *metl-5* (reverse 2), ACCAGGCCGAACCATTTGAA. The results were expressed as $2^{[-(\text{target number of cycles} - \text{actin number of cycles})]}$. Control PCRs were also performed on total RNA that had not been reverse-transcribed to test for the presence of genomic DNA in the RNA preparation.

ORO staining

Briefly, worms were synchronized by egg laying and grown to the L4 stage at 20°C. Worms were washed off plates in 2 ml of PBST solution and spun at 560*g* for 1 min, and supernatant was removed. Worms were washed three times in PBST, and all supernatant save for 100 μl was removed. A total of 600 μl of 40% isopropanol was added, and worms were rocked at room temperature for 3 min. Worms were spun at 560*g* for 1 min, and all but 100 μl of supernatant was removed. ORO working solution (600 μl) was added to each tube. To make a working solution of ORO, initially, 500 mg of ORO powder was added to 100 ml of 100% isopropanol; this stock solution was diluted in water to 60% isopropanol and filtered through a 0.2-μm filter. Worms and working solution of ORO were rocked for 2 hours at room temperature. Tubes were spun at 560*g* for 1 min, and supernatant was removed. Pellets were resuspended in 600 μl of PBST and rotated at room temperature for 30 min. Tubes were centrifuged at 560*g* for 1 min, and supernatant was removed. Five microliters of worms was placed on microscope slides, and a coverslip was added. Slides were imaged on a Zeiss Discovery V8 fluorescent scope, and ORO staining was quantified in ImageJ.

GC-MS quantification of eicosanoids

GC-MS was performed by the Harvard Small Molecule Mass Spectrometry Facility. Briefly, 50 μl of 2-μl 20-HETE-d6 (Cayman Chemical) in methanol was added to each frozen sample as an internal standard to ensure that extractions were equivalent in each sample. Hydrolysis solution (1 ml; 90% methanol in water and 0.3 N KOH) was added to each sample, which was thawed and vortexed. Samples were transferred to bead beater vials with 100 μl of 0.1-mm zirconia beads. Samples were homogenized in a TissueLyser LT at 50 Hz for 15 min. The homogenate (without the beads) was transferred to glass vials and incubated at 80°C for 1 hour before being transferred to Eppendorf tubes and centrifuged at maximum speed for 5 min. The supernatant was transferred to new glass vials and evaporated under N_2 flow, and then, samples were resuspended in 2 ml of 0.1 M ammonium acetate (pH 7.0) and 5% methanol in water and purified by solid-phase extraction (SPE) purification. The hydrolyzed samples were brought to a pH of 6.0 with 25 μl of acetic acid. SPE cartridges (SiliCycle SiliaPrep C8/SAX; 200 mg) were conditioned with 2 ml of methanol followed by 2 ml of 0.1 M ammonium acetate (pH 7.0) and 5% methanol in water. Samples were passed on the cartridges, which were then washed with 2 ml of 50% methanol in water. Samples were eluted with 2 ml of hexane:ethyl acetate 75:25 and 1% acetic acid. Samples were reduced to 1 ml by N_2 flow and transferred to 1.5-ml vials before being evaporated to dryness under N_2 flow. Samples were resuspended in 50 μl of methanol and transferred to glass microinserts. Hydrolysis was adapted from (*56*), and SPE purification was adapted from (*57*). Samples were run on a Thermo Fisher Scientific Q Exactive Plus with a Kinetex 2.6-μm C18 100 Å, 150 × 2.1 mm. Sample (5 μl) was injected, and the column was maintained at 25°C

[polarity +: full MS, 0 to 25 min; resolution, 35,000; AGC (automatic gain control) target, 4×10^5; maximum injection time (max IT), 10 ms; *mz* (mass/charge ratio) range, 250 to 450; polarity −: full MS, 0 to 25 min; resolution, 70,000; AGC target, 1×10^6; max IT, 100 ms; *mz* range, 250 to 450; selective ion monitoring on each compound $[M\text{-}H]^-$; resolution, 35,000; AGC target, 1×10^6; max IT, 50 ms; isolation, 1.5 *mz*; isolation offset, 0.5 *mz*]. Buffer A was 10 mM ammonium acetate, and buffer B was acetonitrile with a flow rate of 0.2 ml/min. The general method and LC method were adapted from (*35*). Pure standards of 20-HEPE, 17,18-EpETE, 17,18-DiHETE, 20-HETE-d6, AA, and EPA (Cayman Chemical) were run to identify retention times. Lipid concentration was normalized to the internal standard in each sample. Standard tests revealed that close to 100% of the standards for 20-HEPE, 17,18-EpETE, and 17,18-DiHETE were recovered, while 50 to 60% of EPA and AA were recovered. Therefore, comparisons were only performed between the same compounds between samples. Other major fatty acids were detected, but their identification was projected on the basis of the accurate mass rather than the running of standards, as was performed for 20-HEPE, 17,18-EpETE, 17,18-DiHETE, 20-HETE-d6, AA, and EPA.

Lipid supplementation

NGM plates were prepared as in (*58*). Briefly, NGM plates were prepared with the addition of 0.1% Tergitol dissolved in water, and eicosanoids or PUFAs were added to the media when it cooled to 55°C. Final concentrations of 1 mM AA, 1 mM EPA, 100 μM 17,18-EpETE, 100 μM 17,18-DiHETE, and 100 μM 20-HEPE were used after initial optimization experiments were performed with concentrations ranging from 10 μM to 1 mM for AA and EPA and 10 to 100 μM for 17,18-EpETE, 17,18-DiHETE, and 20-HEPE based on an examination of lipid concentrations used in previously published papers. Plates were kept in the dark and spotted 24 to 48 hours before L4 worms were added. Worms were grown on supplemented plates for 4 hours before heat shock at 37°C was performed as above. Tergitol alone plates were used as a control.

SUPPLEMENTARY MATERIALS

Supplementary material for this article is available at http://advances.sciencemag.org/cgi/content/full/6/17/eaaz4370/DC1

View/request a protocol for this paper from *Bio-protocol*.

REFERENCES AND NOTES

1. S. Ramagopal, H. L. Ennis, Regulation of synthesis of cell-specific ribosomal proteins during differentiation of *Dictyostelium discoideum*. *Proc. Natl. Acad. Sci. U.S.A.* **78**, 3083–3087 (1981).
2. D. Simsek, G. C. Tiu, R. A. Flynn, G. W. Byeon, K. Leppek, A. F. Xu, H. Y. Chang, M. Barna, The mammalian ribo-interactome reveals ribosome functional diversity and heterogeneity. *Cell* **169**, 1051–1065.e18 (2017).
3. M. M. Parks, C. M. Kurylo, R. A. Dass, L. Bojmar, D. Lyden, C. T. Vincent, S. C. Blanchard, Variant ribosomal RNA alleles are conserved and exhibit tissue-specific expression. *Sci. Adv.* **4**, eaao0665 (2018).
4. N. R. Genuth, M. Barna, The discovery of ribosome heterogeneity and its implications for gene regulation and organismal life. *Mol. Cell* **71**, 364–374 (2018).
5. K. E. Sloan, A. S. Warda, S. Sharma, K.-D. Entian, D. L. J. Lafontaine, M. T. Bohnsack, Tuning the ribosome: The influence of rRNA modification on eukaryotic ribosome biogenesis and function. *RNA Biol.* **14**, 1138–1152 (2017).
6. G. McColl, A. N. Rogers, S. Alavez, A. E. Hubbard, S. Melov, C. D. Link, A. I. Bush, P. Kapahi, G. J. Lithgow, Insulin-like signaling determines survival during stress via posttranscriptional mechanisms in C. elegans. *Cell Metab.* **12**, 260–272 (2010).
7. D. Shenton, J. B. Smirnova, J. N. Selley, K. Carroll, S. J. Hubbard, G. D. Pavitt, M. P. Ashe, C. M. Grant, Global translational responses to oxidative stress impact upon multiple levels of protein synthesis. *J. Biol. Chem.* **281**, 29011–29021 (2006).
8. M. V. Gerashchenko, A. V. Lobanov, V. N. Gladyshev, Genome-wide ribosome profiling reveals complex translational regulation in response to oxidative stress. *Proc. Natl. Acad. Sci. U.S.A.* **109**, 17394–17399 (2012).
9. A. Basu, P. Das, S. Chaudhuri, E. Bevilacqua, J. Andrews, S. Barik, M. Hatzoglou, A. A. Komar, B. Mazumder, Requirement of rRNA methylation for 80S ribosome assembly on a cohort of cellular internal ribosome entry sites. *Mol. Cell. Biol.* **31**, 4482–4499 (2011).
10. M. Schosserer, N. Minois, T. B. Angerer, M. Amring, H. Dellago, E. Harreither, A. Calle-Perez, A. Pircher, M. P. Gerstl, S. Pfeifenberger, C. Brandl, M. Sonntagbauer, A. Kriegner, A. Linder, A. Weinhäusel, T. Mohr, M. Steiger, D. Mattanovich, M. Rinnerthaler, T. Karl, S. Sharma, K.-D. Entian, M. Kos, M. Breitenbach, I. B. H. Wilson, N. Polacek, R. Grillari-Voglauer, L. Breitenbach-Koller, J. Grillari, Methylation of ribosomal RNA by NSUN5 is a conserved mechanism modulating organismal lifespan. *Nat. Commun.* **6**, 6158 (2015).
11. A. C. Kendall, A. Nicolaou, Bioactive lipid mediators in skin inflammation and immunity. *Prog. Lipid Res.* **52**, 141–164 (2013).
12. X. Ye, K. Hama, J. J. A. Contos, B. Anliker, A. Inoue, M. K. Skinner, H. Suzuki, T. Amano, G. Kennedy, H. Arai, J. Aoki, J. Chun, LPA_3-mediated lysophosphatidic acid signalling in embryo implantation and spacing. *Nature* **435**, 104–108 (2005).
13. C. D. Funk, Prostaglandins and leukotrienes: Advances in eicosanoid biology. *Science* **294**, 1871–1875 (2001).
14. J. Hu, T. Frömel, I. Fleming, Angiogenesis and vascular stability in eicosanoids and cancer. *Cancer Metastasis Rev.* **37**, 425–438 (2018).
15. L. M. Iyer, D. Zhang, L. Aravind, Adenine methylation in eukaryotes: Apprehending the complex evolutionary history and functional potential of an epigenetic modification. *Bioessays* **38**, 27–40 (2016).
16. G. Blobel, V. R. Potter, Studies on free and membrane-bound ribosomes in rat liver: I. Distribution as related to total cellular RNA. *J. Mol. Biol.* **26**, 279–292 (1967).
17. N. van Tran, F. G. M. Ernst, B. R. Hawley, C. Zorbas, N. Ulryck, P. Hackert, K. E. Bohnsack, M. T. Bohnsack, S. R. Jaffrey, M. Graille, D. L. J. Lafontaine, The human 18S rRNA m^6A methyltransferase METTL5 is stabilized by TRMT112. *Nucleic Acids Res.* **47**, 7719–7733 (2019).
18. B. E. Maden, Identification of the locations of the methyl groups in 18 S ribosomal RNA from *Xenopus laevis* and man. *J. Mol. Biol.* **189**, 681–699 (1986).
19. Y. S. Polikanov, S. V. Melnikov, D. S öll, T. A. Steitz, Structural insights into the role of rRNA modifications in protein synthesis and ribosome assembly. *Nat. Struct. Mol. Biol.* **22**, 342–344 (2015).
20. P. V. Sergiev, N. A. Aleksashin, A. A. Chugunova, Y. S. Polikanov, O. A. Dontsova, Structural and evolutionary insights into ribosomal RNA methylation. *Nat. Chem. Biol.* **14**, 226–235 (2018).
21. X. Zhao, Y.-T. Yu, Detection and quantitation of RNA base modifications. *RNA* **10**, 996–1002 (2004).
22. L. M. Iyer, S. Abhiman, L. Aravind, Chapter 2—Natural history of eukaryotic DNA methylation systems. *Prog. Mol. Biol. Transl. Sci.* **101**, 25–104 (2011).
23. M.-W. Tan, S. Mahajan-Miklos, F. M. Ausubel, Killing of *Caenorhabditis elegans* by *Pseudomonas aeruginosa* used to model mammalian bacterial pathogenesis. *Proc. Natl. Acad. Sci. U.S.A.* **96**, 715–720 (1999).
24. K. C. Reddy, E. C. Andersen, L. Kruglyak, D. H. Kim, A polymorphism in *npr-1* is a behavioral determinant of pathogen susceptibility in *C. elegans*. *Science* **323**, 382–384 (2009).
25. N. Ishii, K. Takahashi, S. Tomita, T. Keino, S. Honda, K. Yoshino, K. Suzuki, A methyl viologen-sensitive mutant of the nematode *Caenorhabditis elegans*. *Mutat. Res.* **237**, 165–171 (1990).
26. A. Ohta, T. Ujisawa, S. Sonoda, A. Kuhara, Light and pheromone-sensing neurons regulates cold habituation through insulin signalling in *Caenorhabditis elegans*. *Nat. Commun.* **5**, 4412 (2014).
27. S. Murakami, T. E. Johnson, A genetic pathway conferring life extension and resistance to UV stress in Caenorhabditis elegans. *Genetics* **143**, 1207–1218 (1996).
28. B. A. Scott, M. S. Avidan, C. M. Crowder, Regulation of hypoxic death in *C. elegans* by the insulin/IGF receptor homolog DAF-2. *Science* **296**, 2388–2391 (2002).
29. X. Li, O. Matilainen, C. Jin, K. M. Glover-Cutter, C. I. Holmberg, T. K. Blackwell, Specific SKN-1/Nrf stress responses to perturbations in translation elongation and proteasome activity. *PLOS Genet.* **7**, e1002119 (2011).
30. M. Hansen, S. Taubert, D. Crawford, N. Libina, S.-J. Lee, C. Kenyon, Lifespan extension by conditions that inhibit translation in *Caenorhabditis elegans*. *Aging Cell* **6**, 95–110 (2007).
31. N. T. Ingolia, S. Ghaemmaghami, J. R. S. Newman, J. S. Weissman, Genome-wide analysis in vivo of translation with nucleotide resolution using ribosome profiling. *Science* **324**, 218–223 (2009).
32. J. G. Wallis, J. L. Watts, J. Browse, Polyunsaturated fatty acid synthesis: What will they think of next? *Trends Biochem. Sci.* **27**, 467–473 (2002).
33. K. A. Massey, A. Nicolaou, Lipidomics of polyunsaturated-fatty-acid-derived oxygenated metabolites. *Biochem. Soc. Trans.* **39**, 1240–1246 (2011).
34. E. H. Oliw, Oxygenation of polyunsaturated fatty acids by cytochrome P450 monooxygenases. *Prog. Lipid Res.* **33**, 329–354 (1994).

35. J. Kulas, C. Schmidt, M. Rothe, W. H. Schunck, R. Menzel, Cytochrome P450-dependent metabolism of eicosapentaenoic acid in the nematode *Caenorhabditis elegans*. *Arch. Biochem. Biophys.* **472**, 65–75 (2008).
36. Y. Zhou, J. R. Falck, M. Rothe, W.-H. Schunck, R. Menzel, Role of CYP eicosanoids in the regulation of pharyngeal pumping and food uptake in *Caenorhabditis elegans*. *J. Lipid Res.* **56**, 2110–2123 (2015).
37. R. W. French, Notes on technic. *Stain Technol.* **1**, 78–80 (1926).
38. F. Proescher, Oil red O pyridin, a rapid fat stain. *Stain Technol.* **2**, 60–61 (1927).
39. D. K. Ma, M. Rothe, S. Zheng, N. Bhatla, C. L. Pender, R. Menzel, H. R. Horvitz, Cytochrome P450 drives a HIF-regulated behavioral response to reoxygenation by *C. elegans*. *Science* **341**, 554–558 (2013).
40. H. D. Hoang, J. K. Prasain, D. Dorand, M. A. Miller, A heterogeneous mixture of F-series prostaglandins promotes sperm guidance in the *Caenorhabditis elegans* reproductive tract. *PLOS Genet.* **9**, e1003271 (2013).
41. M. Deline, J. Keller, M. Rothe, W.-H. Schunck, R. Menzel, J. L. Watts, Epoxides derived from dietary dihomo-gamma-linolenic acid induce germ cell death in *C. elegans*. *Sci. Rep.* **5**, 15417 (2015).
42. B. Gerisch, C. Weitzel, C. Kober-Eisermann, V. Rottiers, A. Antebi, A hormonal signaling pathway influencing *C. elegans* metabolism, reproductive development, and life span. *Dev. Cell* **1**, 841–851 (2001).
43. K. Jia, P. S. Albert, D. L. Riddle, DAF-9, a cytochrome P450 regulating *C. elegans* larval development and adult longevity. *Development* **129**, 221–231 (2002).
44. D. L. Motola, C. L. Cummins, V. Rottiers, K. K. Sharma, T. Li, Y. Li, K. Suino-Powell, H. E. Xu, R. J. Auchus, A. Antebi, D. J. Mangelsdorf, Identification of ligands for DAF-12 that govern dauer formation and reproduction in *C. elegans*. *Cell* **124**, 1209–1223 (2006).
45. W. Jiang, Y. Wei, Y. Long, A. Owen, B. Wang, X. Wu, S. Luo, Y. Dang, D. K. Ma, A genetic program mediates cold-warming response and promotes stress-induced phenoptosis in *C. elegans*. *eLife* **7**, (2018).
46. H. Ma, X. Wang, J. Cai, Q. Dai, S. K. Natchiar, R. Lv, K. Chen, Z. Lu, H. Chen, Y. G. Shi, F. Lan, J. Fan, B. P. Klaholz, T. Pan, Y. Shi, C. He, N^{6}-Methyladenosine methyltransferase ZCCHC4 mediates ribosomal RNA methylation. *Nat. Chem. Biol.* **15**, 88–94 (2019).
47. S. Brenner, The genetics of *Caenorhabditis elegans*. *Genetics* **77**, 71–94 (1974).
48. C. C. Mello, J. M. Kramer, D. Stinchcomb, V. Ambros, Efficient gene transfer in C.elegans: Extrachromosomal maintenance and integration of transforming sequences. *EMBO J.* **10**, 3959–3970 (1991).
49. E. L. Greer, D. Dowlatshahi, M. R. Banko, J. Villen, K. Hoang, D. Blanchard, S. P. Gygi, A. Brunet, An AMPK-FOXO pathway mediates longevity induced by a novel method of dietary restriction in *C. elegans*. *Curr. Biol.* **17**, 1646–1656 (2007).
50. F. Aeschimann, J. Xiong, A. Arnold, C. Dieterich, H. Großhans, Transcriptome-wide measurement of ribosomal occupancy by ribosome profiling. *Methods* **85**, 75–89 (2015).
51. M. V. Gerashchenko, V. N. Gladyshev, Ribonuclease selection for ribosome profiling. *Nucleic Acids Res.* **45**, e6 (2017).
52. M. Martin, Cutadapt removes adapter sequences from high-throughput sequencing reads. *EMBnet.journal* **17**, 10.14806/ej.17.1.200, (2011).
53. A. Dobin, C. A. Davis, F. Schlesinger, J. Drenkow, C. Zaleski, S. Jha, P. Batut, M. Chaisson, T. R. Gingeras, STAR: Ultrafast universal RNA-seq aligner. *Bioinformatics* **29**, 15–21 (2013).
54. M. I. Love, W. Huber, S. Anders, Moderated estimation of fold change and dispersion for RNA-seq data with DESeq2. *Genome Biol.* **15**, 550 (2014).
55. A. Subramanian, P. Tamayo, V. K. Mootha, S. Mukherjee, B. L. Ebert, M. A. Gillette, A. Paulovich, S. L. Pomeroy, T. R. Golub, E. S. Lander, J. P. Mesirov, Gene set enrichment analysis: A knowledge-based approach for interpreting genome-wide expression profiles. *Proc. Natl. Acad. Sci. U.S.A.* **102**, 15545–15550 (2005).
56. S. Tumanov, V. Bulusu, J. J. Kamphorst, Analysis of fatty acid metabolism using stable isotope tracers and mass spectrometry. *Methods Enzymol.* **561**, 197–217 (2015).
57. J. Rivera, N. Ward, J. Hodgson, I. B. Puddey, J. R. Falck, K. D. Croft, Measurement of 20-hydroxyeicosatetraenoic acid in human urine by gas chromatography-mass spectrometry. *Clin. Chem.* **50**, 224–226 (2004).
58. M. L. Deline, T. L. Vrablik, J. L. Watts, Dietary supplementation of polyunsaturated fatty acids in *Caenorhabditis elegans*. *J. Vis. Exp.* , (2013).

Acknowledgments: We thank members of the Greer lab, J. Lieberman, K. Blackwell, and A. Brunet for discussions and feedback on the manuscript. We thank M. Bland, Z. Wu, and K. Blackwell for providing RNAi clones and PA14 bacteria; M. Hansen for protocol information on ^{35}S-methioinine feeding experiments; C. Serhan for advice about eicosanoids; A. Lanjuin, S. Duhta, and W. Mair for pSD1 plasmid; and C. Vidoudez at the Small Molecule Mass Spectrometry Facility at Harvard University for the extraction and GC-MS analysis of lipids. **Funding:** Z.K.O. was supported by T32-HD007466. S.Y.W. was supported by a Croucher fellowship. This work was supported by NIH grants (R00AG043550, DP2AG055947, and R21HG010066) and an American Federation for Aging Research grant (A16044) to E.L.G.
Author contributions: N.L., Z.K.O. and E.L.G. conceived and planned the study. E.L.G. wrote the paper. Z.K.O. produced Figs. 1 (A, B, D, and E) and 3A and figs. S1B and S3 (A, B, and D). N.L. performed ribosome profiling, RNA sequencing experiments, and cloning for transgenic lines and produced Figs. 3F and 4 (C and H) and figs. S1C, S2J, S4D, and S6 (B and C). A.S.E. produced Figs. 1B, 2 (A and B), and 4B and fig. S3 (B to H). K.B. produced Fig. 1F and fig. S1A and generated all transgenic lines. M.V.G. performed RNA sequencing analysis and ribosome sequencing analysis and produced Fig. 4 (D to F) and figs. S4 and S5. S.Y.W. performed RNA sequencing analysis and produced fig. S3 (I and J). C.F. produced fig. S3 (I and J). P.-E.F. helped produce fig. S3 (A, B, and D). V.N.G. advised M.V.G. E.L.G. produced Figs. 2C, 3 (A to E, G, and I), 4 (A, B, and G), and 5 and figs. S2 (A to I), S6A, and S7. All authors discussed the results and commented on the manuscript. **Competing interests:** The authors declare that they have no competing interests. **Data and materials availability:** All data needed to evaluate the conclusions in the paper are present in the paper and/or the Supplementary Materials. Detailed analytical pipeline and all custom scripts are openly available on GitHub (https://github.com/germaximus/Liberman_2019). Raw data and gene counts tables are available from the NCBI Gene Expression Omnibus repository under accession number GSE131269. Additional data related to this paper may be requested from the authors.

Submitted 9 September 2019
Accepted 27 January 2020
Published 22 April 2020
10.1126/sciadv.aaz4370

Citation: N. Liberman, Z. K. O'Brown, A. S. Earl, K. Boulias, M. V. Gerashchenko, S. Y. Wang, C. Fritsche, P.-E. Fady, A. Dong, V. N. Gladyshev, E. L. Greer, N6-adenosine methylation of ribosomal RNA affects lipid oxidation and stress resistance. *Sci. Adv.* **6**, eaaz4370 (2020).

Science Advances

N6-adenosine methylation of ribosomal RNA affects lipid oxidation and stress resistance

Noa Liberman, Zach K. O'Brown, Andrew Scott Earl, Konstantinos Boulias, Maxim V. Gerashchenko, Simon Yuan Wang, Colette Fritsche, Paul-Enguerrand Fady, Anna Dong, Vadim N. Gladyshev and Eric Lieberman Greer

Sci Adv **6** (17), eaaz4370.
DOI: 10.1126/sciadv.aaz4370

Science Advances (ISSN 2375-2548) is published by the American Association for the Advancement of Science, 1200 New York Avenue NW, Washington, DC 20005. The title *Science Advances* is a registered trademark of AAAS.